Clockwork Orangutan: microRNAs, thermoregulatory tradeoffs, and the evolution of brain size

Bastian Fromm, PhD**
UiT - The Arctic University of Norway,
The Arctic University Museum of Norway
9006 Tromsø, NO

Thomas Sorger, PhD*
Department of Biology
Roger Williams University
Bristol, RI 02809

*** Lead contact**
****Second corresponding author**

SUMMARY

The advent of placentation and permanent homeothermy depended on major increases in metabolic rates and coincided with expansions in the number of microRNA families (*mirFam*). Since models of the evolution of brain size in the human lineage have not accounted for thermoregulatory constraints, we reparametrized rates of energy expenditure from log-based specific *MR*s to *mirFam*-based cellular *MR*s (*cMR*s). We demonstrate that mammalian brain and liver sizes vary inversely relative to a thermoregulatory Core (kidney+heart+liver+brain). Liver *cMR*s also vary inversely with respect to body mass and the *cMR*s of kidney, heart and brain, recapitulating the downregulation of gluconeogenesis during developmental growth of whole body and liver. With *mirFam* as a proxy for energy reliability, a logistic feedback model of relative brain size detected adaptation to a low-energy regime among the smallest primates and, among the largest primates, adaptation to the physiological limit on the rate of heat dissipation.

INTRODUCTION

The diversification of mammalian orders is characterized by two long-term trends: increasing size[1] and decreasing body temperature[2]. Resting metabolic rates (*rMR*s) do not exhibit a long-term trend but, in coordination with thermal conductance (C_{min}), allow most orders of mammals to occupy nearly every climatic zone regardless of size[3-4], albeit with a narrower range of tolerance to heat than to cold[5-7]. These observations support the evolutionary relevance of a physiological limit on the rate of heat dissipation, initially proposed by Speakman and Król (2010)[8]. Since current models of the evolution of brain size in the human lineage do not consider thermoregulatory constraints[9-10], there is no satisfactory physiological explanation for the brain's evolutionary expansion. We find that the divergence of Catarrhini coincides with a 15% increase in the median number of microRNA families (*mirFam*), similar to the expansion of *mirFam* associated with the divergence of Boreoeutheria[11] that coincided with faster metabolic rates (*MR*s), higher body temperatures, and the emergence of permanent homeothermy[11]. This adaptive shift to 24-h control of body temperature crossed a threshold of energy reliability relative to earlier-branching placentals and marsupials, among which many orders exhibit some degree of heterothermy[12-13], and set the stage for the subsequent ecological diversification of mammals[14].

Orangutans are similar in body size to humans, but their brains are ⅔ smaller and generate heat at a rate of only 4W, compared to 15W in humans[15]. This raises by 0.2° - 0.3°C the temperature of the brain's venous outflow[16-18], equivalent to 15% of total blood volume per minute[19-20]. Such a

thermoregulatory challenge can be addressed in only two ways: a faster rate of heat dissipation, or a tradeoff in energy expenditure with another metabolically expensive tissue, such as kidney, heart, liver or intestine[21-23]. Like chimpanzees[24], ancestral humans probably relied on behavioral thermoregulation in order to avoid hyperthermia in hot environments which, however, would not have addressed the problem of rapid internal heat generation. Uniquely human adaptations that promoted heat dissipation include hairlessness, bipedalism, and a 10-fold increase in the density of eccrine sweat glands relative to the densities found in chimpanzees and macaques[25]. The latter adaptation may have also increased the risk of dehydration[25] in a drier savannah environment[27-30].

Despite numerous attempts, the effort to detect the tradeoff predicted by the "expensive tissue hypothesis"[22] has been abandoned since the publication of a study encompassing 100 species, including 23 primates, that found no significant anticorrelations among the body mass-independent residuals of eight organs[23]. Lande (1979)[31] first attributed the evolutionary increase in primate brain size to a genetic uncoupling of its dependence on body size. We postulated that thermal homeostasis could be achieved by relaxing the constraint imposed by body size not only on the size of the brain, but also on that of the three other major thermogenic organs (kidney, heart and liver). In this case, the relevant standard for variation of the four most thermogenic organs would the mass of a composite thermogenic "Core", analogous to the thermoregulatory core predicted by the biophysical model of Porter and Kearney (2009)[32]. Relative to this Core, we find that evolutionary increases in the proportion of the brain have been offset by decreases in the proportion of the liver, with a corresponding anticorrelation between their mass-independent residuals.

In order to compare of the evolution of the rates of thermogenesis among these four organs, we estimated their cellular *MR*s (*cMR*s) according to three criteria:

a) correlation with organ size and *mirFam* (physiological relevance)[11];
b) correspondence between the joint *cMR* of the four Core organs and the predicted rate of core thermogenesis (~ $\sqrt{M}$)[32] (thermodynamic relevance);
c) utility for the unsupervised classification of major primate clades (phylogenetic relevance).

We find that liver *cMR*s are anticorrelated with body mass and the *cMR*s of kidney, heart and brain. Allometric scaling of the Core *cMR* ($M^{0.53}$) matches the theoretical rate of core thermogenesis[32], Since the liver is the primary organ of gluconeogenesis during fasting or starvation, this liver-brain anticorrelation is consistent with an energy-limited, positive feedback model of brain size evolution[9-10].

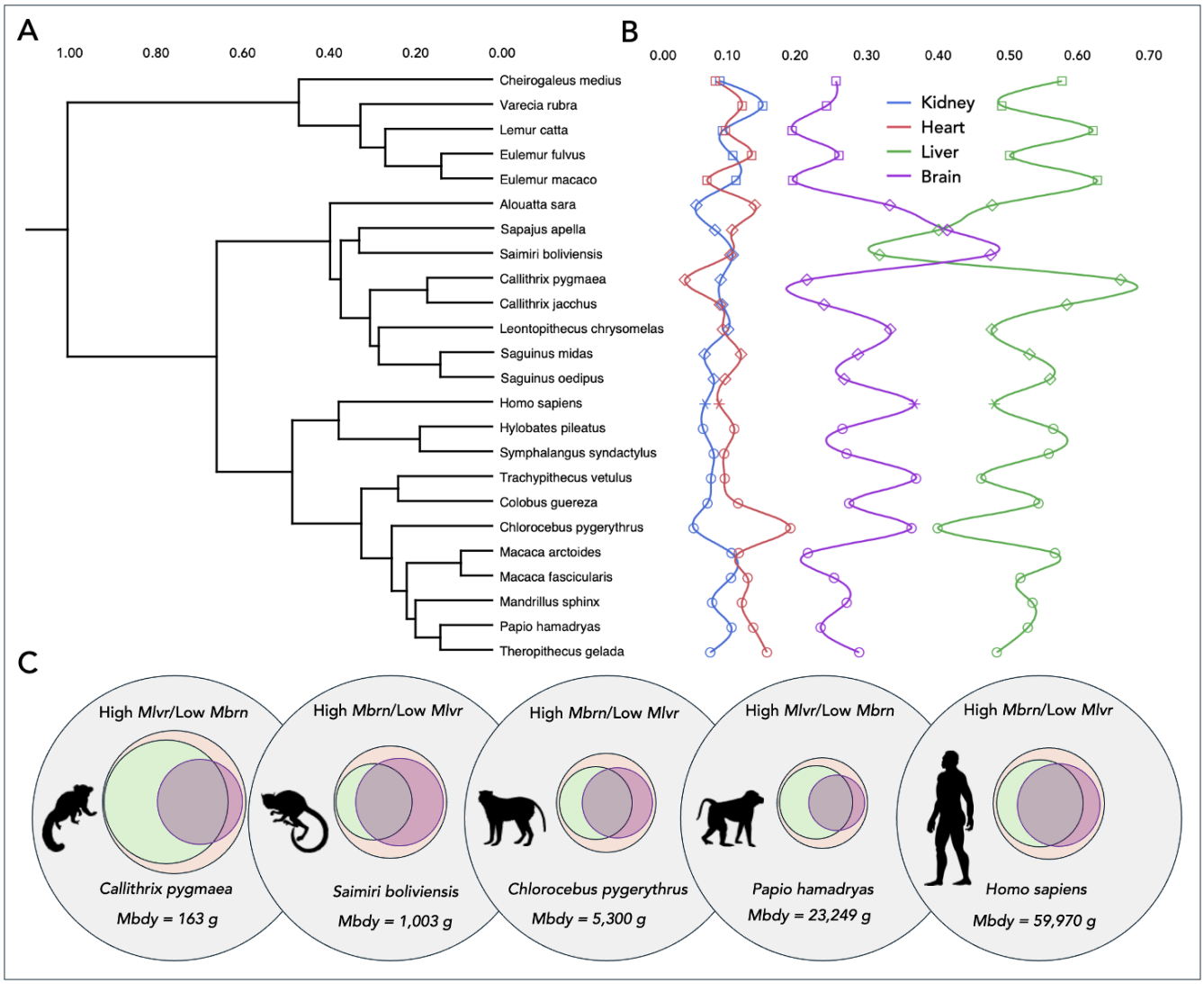

Figure 1. The proportion of brain mass in the Core varies reciprocally with that of the liver.
A. Time tree of 24 primates. The scale bar represents the relative time of divergence.
B. Mass proportion of each organ relative to the total Core mass.
C. Summary model comparing representative species with low or high ratios of brain/liver mass. The radius of each circle represents a spherical volume proportional to organ or Core mass. The relative sizes of liver and brain are represented by green and purple circles, respectively. Silhouttes: *Callithrix jacchus*, *Saimiri* (generic), *Erythrocebus patas*, *Papio* (generic), *Homo sapiens idaltu* (© Phylopic 2024, compiled by T. Michael Keesey).

RESULTS

The proportion of brain mass in the Core varies reciprocally with that of liver

Of six possible tradeoffs among four thermogenic organs, two occurred consistently in primate clades, that between brain and liver (Figure 1A, B), along with a dampened tradeoff between heart and kidney. The same tradeoffs were observed among Glires, Laurasiatheria, Marsupialia, and an Afrotherian. (Supplementary Figures S1 and S2). Two species exhibited unusually high brain/Core ratios: the elephant, with its prehensile trunk, and the arboreal binturong, the only civet with a prehensile tail[33-34].

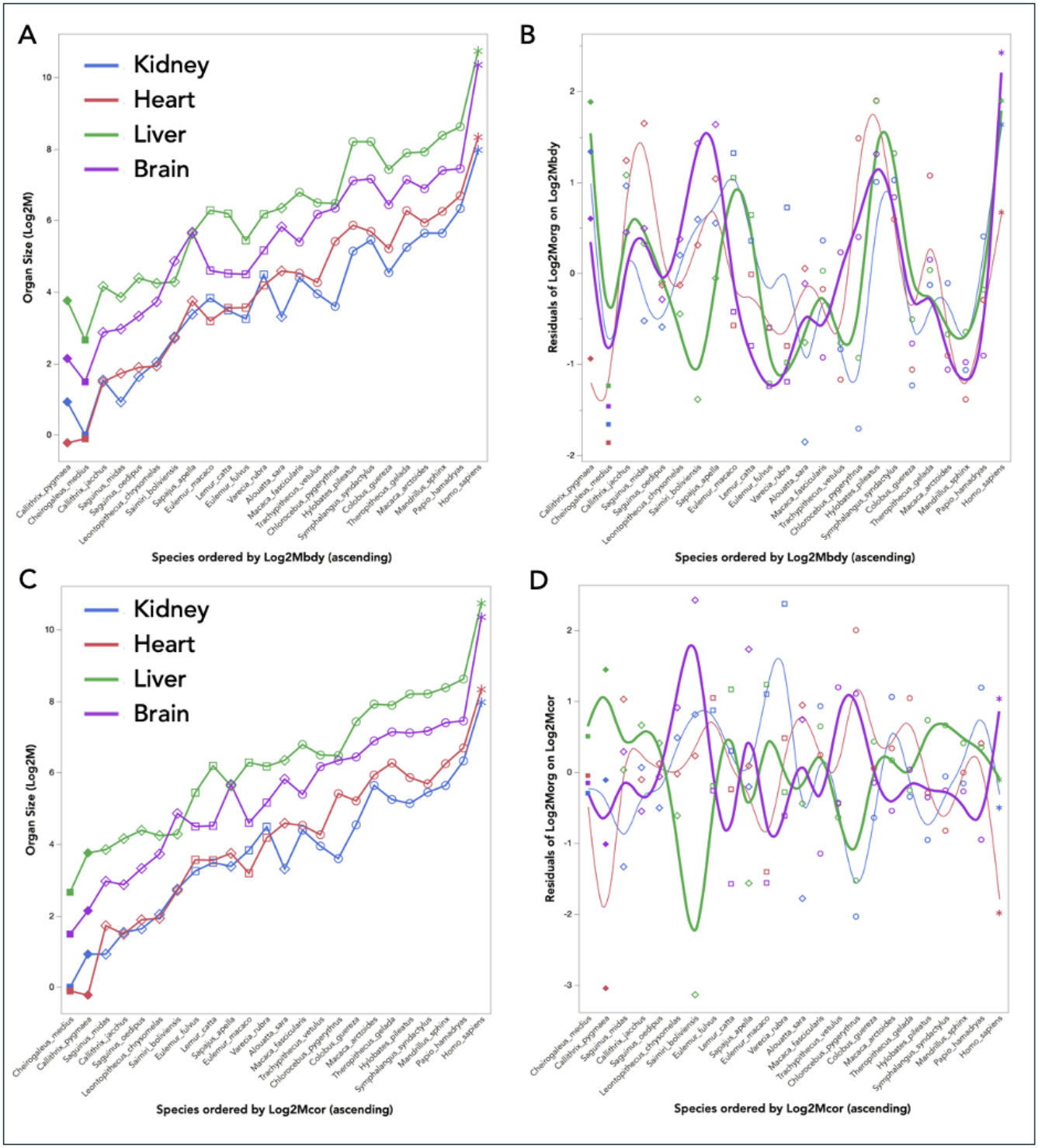

Figure 2. Variation of liver and brain mass relative to the whole body or the Core.
A and C: Variation of organ size relative to body size and Core size in primates (N = 24).
B and D: Mass-independent residual variation relative to body size and Core size in primates.

A tradeoff between liver and brain mass was also readily demonstrable in log-transformed data, provided that they were ranked according to Core size (Figure 2C) rather than body size (Figure 2A). Residuals of mass-independent regressions exhibited a periodic pattern of variation for each organ,

corresponding to the relative proportion of body mass (Figure 2B) or Core mass (Figure 2D). Since the tradeoff between the residuals of brain and liver mass is apparent only when ranked according to Core mass, standardization of log *Mbrn* with respect to log *Mbdy*[23] has precluded its detection.

Physiologically-based cMRs do not correspond to log-based sMRs

Assuming power law models, we distinguish between:

specific *MR* (*sMR*): $sMR = m \times M^b$,

where *b* is the slope of log *rMR*/log *M*, and

cellular *MR* (*cMR*): $cMR = n \times M^c$,

where *c* is the allometric exponent obtained by maximum likelihood fitting of rMR/M^c to the distribution of a physiologically-relevant trait, such as *mirFam*[11]. In the present report, "*rMR*" includes metabolic rates measured under basal conditions (*bMR*s). As previously shown, *mirFam*-based cellular *MR*s (*cMR*s) are sensitive to body temperature and robust to variation in the range of mass, unlike log-based *sMR*s[11]. By definition, an *sMR* has a fixed value regardless of size; thus, the ratio of *sMR* to a non-logarithmic trait that varies with size, such as *mirFam*, is uninformative (Supplementary Figure S3-A). A *mirFam*-based *cMR* increases or decreases as a function of size (Supplementary Figure S3-B), yielding a biologically informative and phylogenetically consistent rank order for *cMR*/trait ratios (Supplementary Figure S4), with significant implications for covariance models of trait evolution[35-38].

Estimation of thermogenic organ cMRs

The context for our method is that the variation of mammalian *cMR* with respect to *mirFam* best fit a model of stabilizing selection when whole-body *cMR* was scaled to $M^{0.75}$ (hence "*cMR.75bdy*")[11]. In order to estimate a *mirFam*-based *cMR* for each thermogenic organ, we compared its dependence on both *mirFam* and organ mass in the range *cMR.60* - *cMR.90*, revealing opposite directions of correlation: increasing *P* values for kidney, heart and brain and decreasing *P* values for liver and whole body (Figure 3). Regression on *mirFam* or binned *mirFam* alone, without correction for organ mass, yielded essentially the same patterns, the only difference being a shift in the peak of the distribution of *P* values for *cMRbdy* from $M^{0.70}$ to $M^{0.75}$ (Supplementary Figure S5). *Assuming an operating range of* $M^{0.70}$ - $M^{0.80}$, we estimated each organ *cMR* based on the lowest *P* value in this range, hence:

*cMR.**70**kdn*, *cMR.**70**hrt*, *cMR.**70**brn* and *cMR.**80**lvr*.

Inspection of Figure 3 reveals that the range $M^{0.70}$ - $M^{0.80}$ defines the limits of a zone of minimal correlation of the Core *cMR* with Core mass and *mirFam*, centered at $M^{0.75}$.

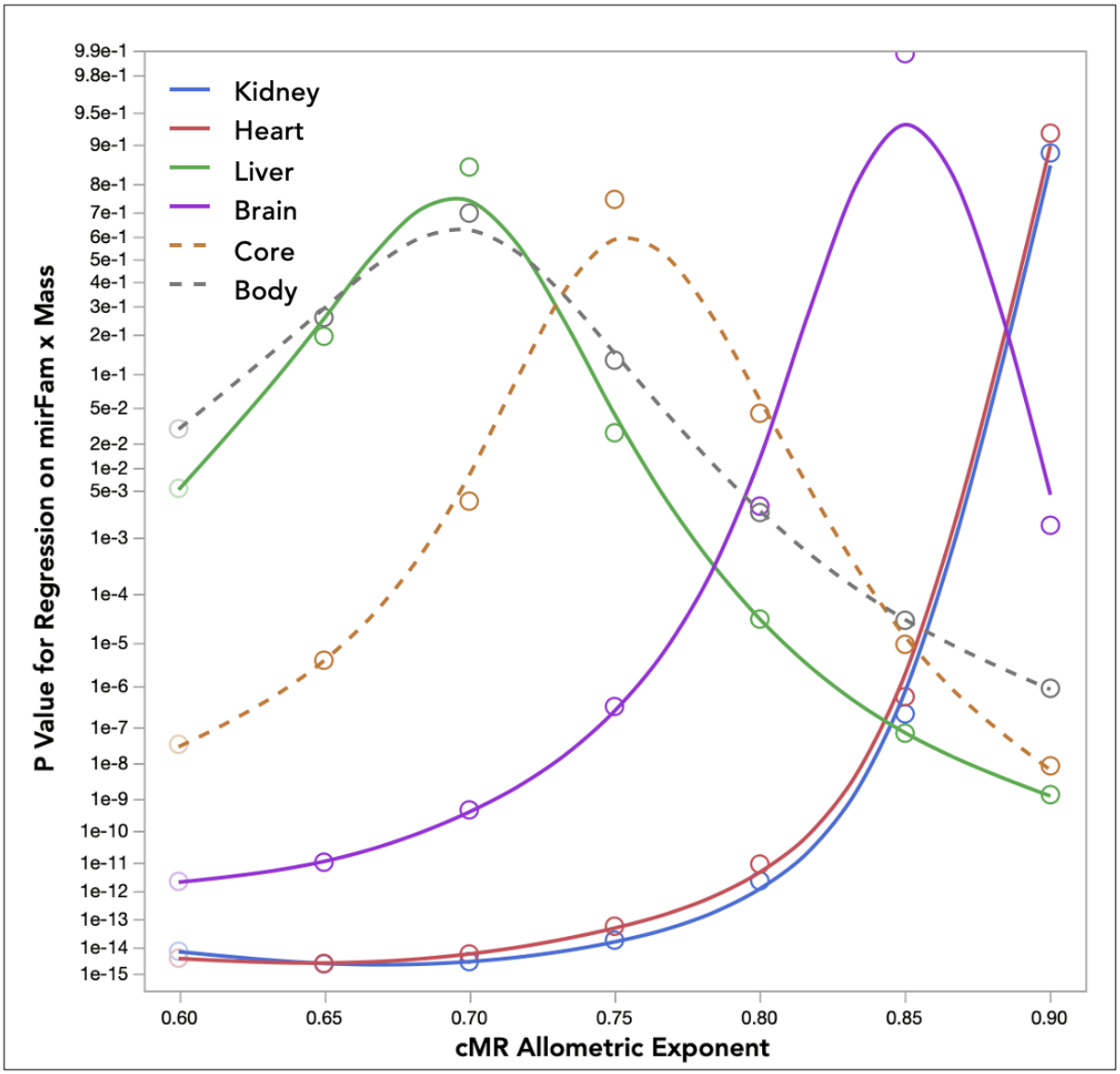

Figure 3. Dependence of *cMR* on *mirFam* and √*Morg* ($Morg^{0.5}$; 51 Euarchontoglires).
P values for regressions of organ *cMR* on √*Morg* and *mirFam* (binned – see Methods).
Regression on √*Morg* yielded *P* values several orders of magnitude lower than regression on log *Morg*.
Note that the minimal correlation for the Core *cMR* occurs when it is scaled to $M^{0.75}$.

For each organ, as shown in Figure 4, the log-based *sMR* occurs at the crossover point for the inversion of the *cMR* slope with respect to organ size, and therefore also of minimal constraint by this factor. Again, there was an obvious distinction between the slope inversions for kidney, heart and brain (~ *cMR.85*) (Figure 4A) and the slope inversions for liver and whole body (~ *cMR.70*) (Figure 4B). Only the Core exhibited an intermediate slope inversion and log-based *sMR* ($M^{0.756}$) (Figure 4B), corresponding to Kleiber's allometric exponent for mammalian *sMR*[39]. $M^{0.75}$ was aslo the optimal scaling for a model of stabilizing selection of mammalian *cMR* with respect to *mirFam*[11], implying that these relationships reflect the outcome of a high degree of evolutionary conservation.

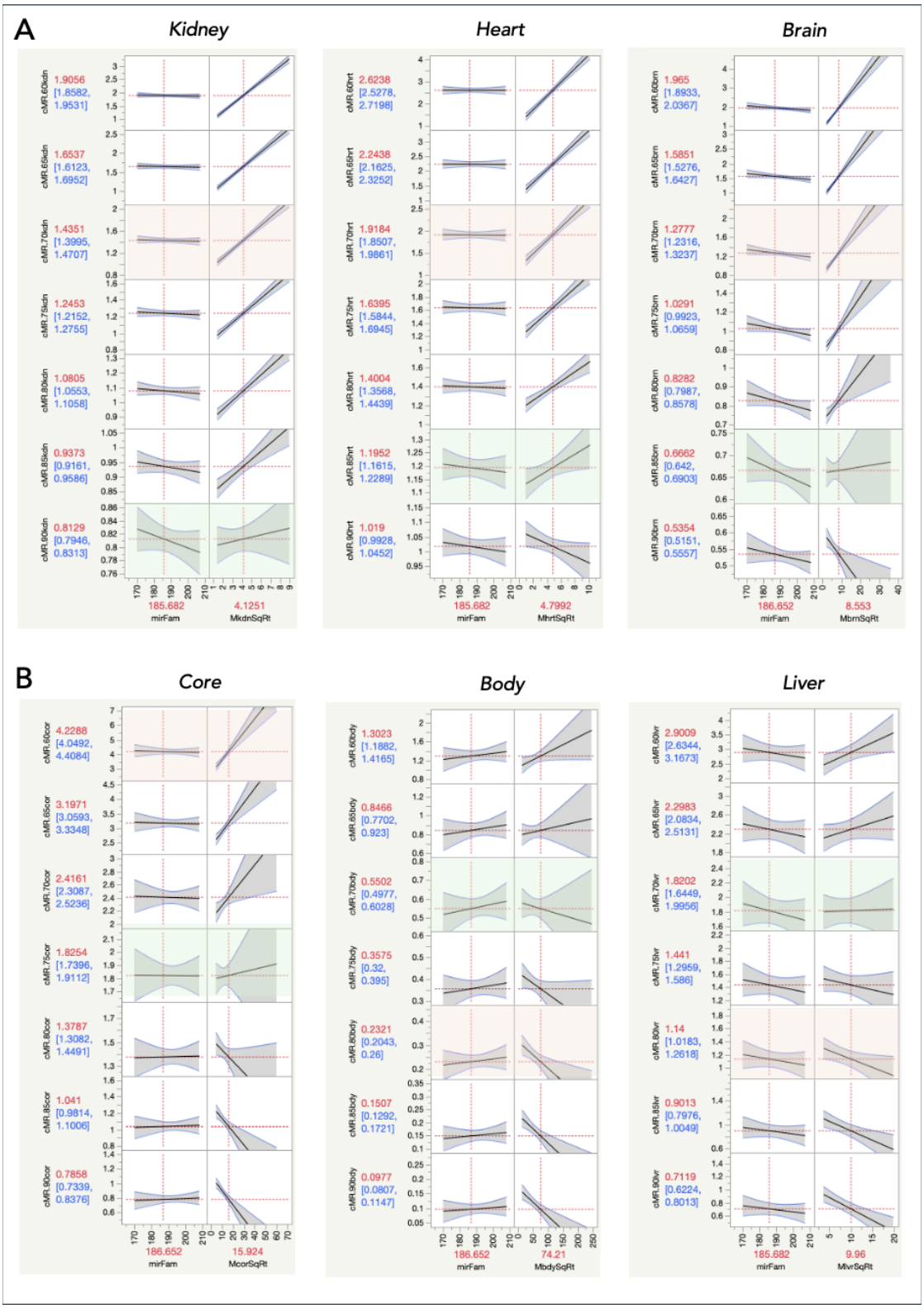

Figure 4. *cMR* slopes with respect to *mirFam* and $\sqrt{M}$, as a function of allometric exponent (22 primates). Estimated *cMR* slopes are shaded pink, log-based *sMR* slopes are shaded green.

Note that log-based *sMR*s correspond to crossover points for the inversions of *cMR* slope with respect to $\sqrt{M}$.

A. Kidney, heart and brain *cMR*s exhibit similar patterns of slope inversion with respect to $\sqrt{M}$.

B. Liver and body *cMR*s exhibit similar slope inversions with respect to $\sqrt{M}$.

Only the Core *cMR* slopes invert at $M^{0.75}$. Values in red represent means ± CI (blue).

Plotting the estimated *cMR*s as a function of primate whole body size revealed a strict anticorrelation between liver *cMR.80 versus* body size and the *cMR.70*s of kidney, heart and brain (Figure 5A). The slightly negative slope for *cMR.75bdy* with respect to log *Mbdy* was not significantly different from 0.0 (P = 8.5e-02). The same ranking of slopes (heart > kidney > brain) and anticorrelation with liver *cMR.80* was obtained when organ *cMR*s were regressed on the thermal conductance (C_{min}) of 21 Boreoeuetheria (Figure 5B), pointing to a common origin for these physiological and thermoregulatory relationships. C_{min} is an extensive property that depends primarily on total body surface area and, secondarily, on the properties of the insulating layer[40]. Ranking 21 Boreoeutheria according to log C_{min} revealed a tradeoff of between the Core mass independent residuals of liver and brain and between *cMR.80lvr* and *cMR.70brn* (Supplementary Figure S6).

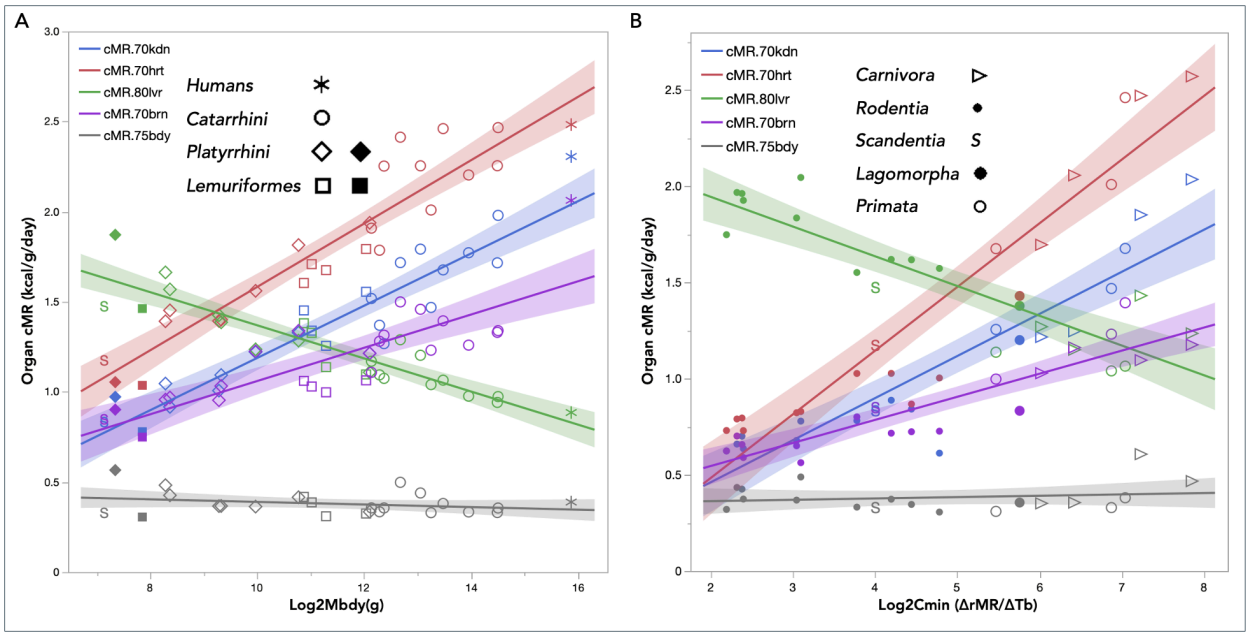

Figure 5. Core organ *cMR*s as a function of body size or thermal conductance.
A. Primates (N = 24). Filled symbols represent likely heterotherms.
B. Boreoeutheria (N = 21). Shaded bands: confidence interval for each regression.

Thermodynamic and phylogenetic relevance of Core organ cMRs

For a steady state (whole animal) resting *MR* that scales as $M^{0.75}$, the rate of core thermogenesis is predicted to scale approximately as $\sqrt{M}$[32]. We applied partial least squares regression[41] in order to predict the optimal scaling of a joint Core *cMR* composed of either *mirFam*-based *cMR*s:

$$cMR.Xcor = (rMRkdn + rMRhrt + rMRlvr + rMRbrn) / (Mkdn + Mhrt + Mlvr + Mbrn)^X$$
$$= (a \bullet cMR.\mathbf{70kdn}) + (b \bullet cMR.\mathbf{70hrt}) + (c \bullet cMR.\mathbf{80lvr}) + (d \bullet cMR.\mathbf{70brn})$$

or log-based *sMR*s:

$$sMR.Xcor = (rMRkdn + rMRhrt + rMRlvr + rMRbrn) / (Mkdn + Mhrt + Mlvr + Mbrn)^X$$
$$= (a' \bullet sMR.\mathbf{90kdn}) + (b' \bullet sMR.\mathbf{87hrt}) + (c' \bullet sMR.\mathbf{67lvr}) + (d' \bullet sMR.\mathbf{83brn})$$

In primates, the composite *cMR* model exhibited two peaks, one on either side of the inversion of *cMR.75cor* slopes with respect to √M: a broad peak centered at $M^{0.53}$, similar to that predicted by the biophysical model of core thermogenesis[32], and a second peak between $M^{0.80}$ - $M^{0.85}$ (Figure 6A). The log-based joint *sMR* model exhibited a single sharp peak at $M^{0.75}$, incompatible with the proposed core-periphery thermodynamic model, which assumes $M^{0.75}$ scaling for whole-body *sMR*[32].

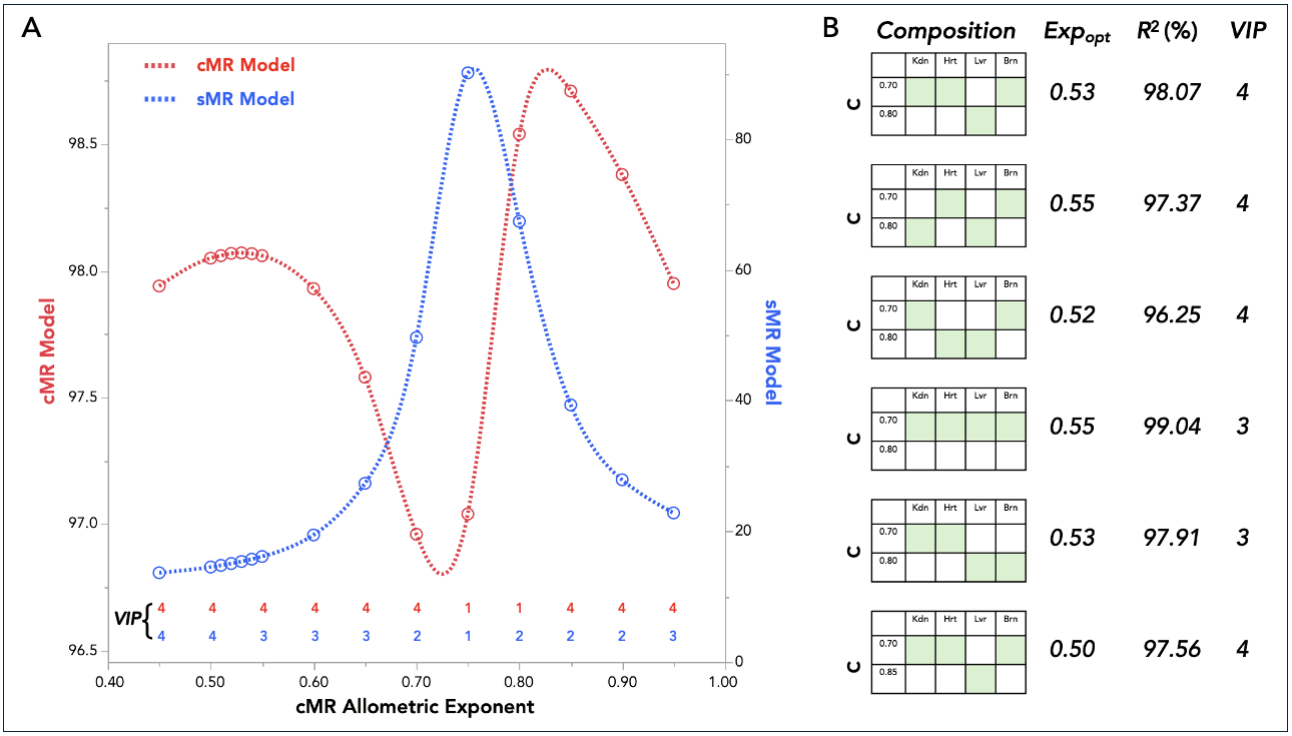

Figure 6. R^2 (% variation) for models of *cMRcor* predicted by linear combinations of the *mirFam*-based *cMR*s or log-based *sMR*s of the four thermogenic organs (note the difference between the scales) (N = 22).
A. Comparison between *mirFam*-based organ *cMR*s and log-based organ *sMR*s.
Below the plot, the table of values for *VIP* (*variable importance of projection*) indicates the number of organs upon which each the model is significantly dependent[42].
B. Comparison of combinations of *cMR.70* and *cMR.80* among the four thermogenic organs.
"c" is the organ *cMR* allometric exponent. "Exp_{opt}" is the optimally fitting allometric exponent of the model.

Importantly, the *cMR* and *sMR* models exhibited critical differences in *VIP* statistics (*Variable Importance of Projection*[42]), a measure of the number of variables constraining each model (Figure 6A, bottom). In the range *cMR.55cor* - *cMR.70cor*, only the *cMR* models depended on all four organ *cMR*s (Figure 6A, bottom). When scaled to $M^{0.75}$, both the *cMR* and *sMR* models of the Core were unconstrained by kidney, heart or brain, depending only on the *cMR* of the liver (Figure 6A, bottom).

We applied an additional test of the relevance of the estimated organ *cMR*s by comparing the joint *cMR*s obtained by permuting the combinations of the estimated organ *cMR*s, yielding four models with *VIP* = 4 (Figure 6B). Of these combinations, we found two that were able to resolve Platyrrhini from Lemuriformes in an unsupervised classification of major primate clades[43]: either *cMR.80* or *cMR.85* for liver, together with *cMR.70*s for heart, kidney and brain. When liver *cMR* was varied between *cMR.75* - *cMR.85*, the lowest value for the Bayes information criterion (BIC) corresponded to the originally estimated set of *mirFam*-based *cMR*s (Supplementary Figure S7), yielding the following optimal primate model of thermogenesis by the defined, 4-organ Core:

cMR.53*cor** = 0.53 • ***cMR.70kdn + 0.69 • ***cMR.70hrt*** + 0.37 • ***cMR.80lvr*** + 0.09 • ***cMR.70brn***

In the context of the evolution of thermoregulation, the coefficient of each organ *cMR* in this model indicates its relative impact on the total rate of internal thermogenesis, from which one can infer the degree to which it has been constrained by natural selection *i.e.* the smaller its coefficient, the greater the degree of permitted evolutionary variation of the organ *cMR* since clade divergence..

Comparison of the parameters of Core *cMR* models among three different orders of Boreoeutheria sheds light on the history of thermoregulatory adaptations (Figure 7).

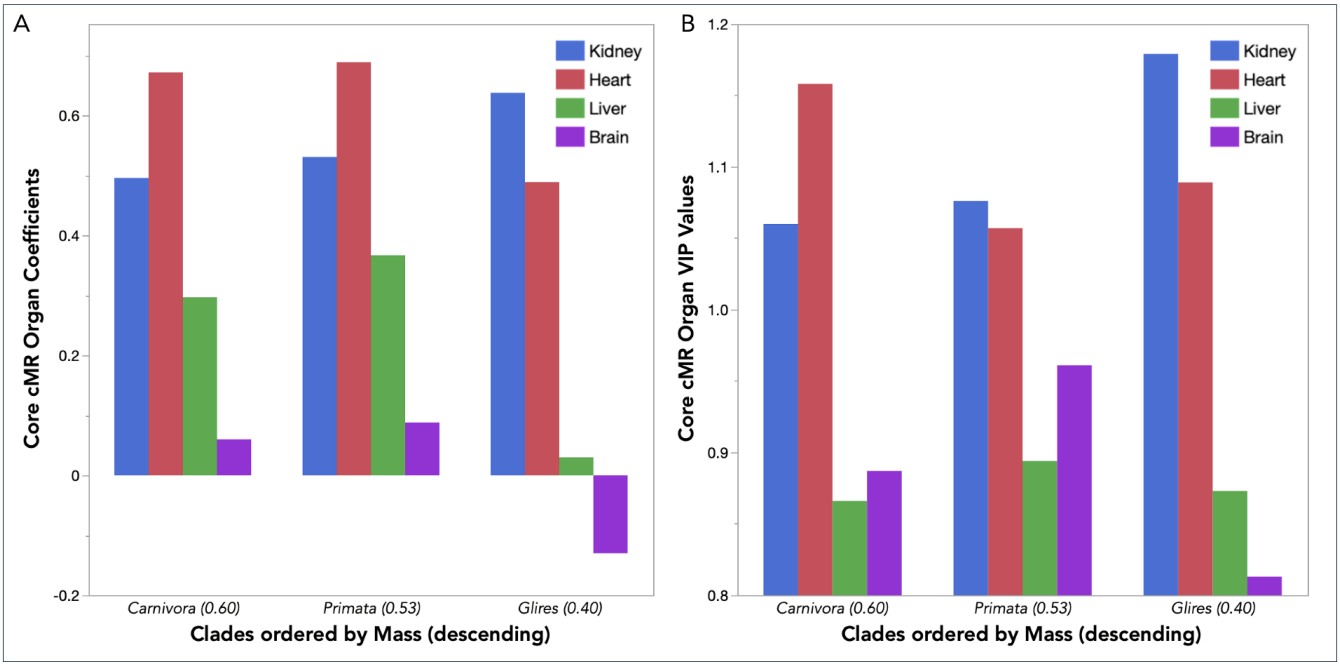

Figure 7. Organ cMR coefficients and VIP values for Core models in Boreoeutheria.
Values in parentheses next to each clade indicate the optimal allometric exponent of the Core *cMR* model.
A. Organ coefficients for the optimal model for Carnivora (N = 30), Primate (N = 22) and Glires (N = 26).
B. Organ VIP values above threshold of significance (0.80) for each model.

The original biophysical model for thermogenesis assumed that metabolic heat emanates from the geometric center of an ellipsoid endotherm[32]. Depending on the wind condition or the presence of fur, the authors derived a single allometric exponent between 0.46 - 0.58 to scale the rate of thermogenesis across the entire range of mammalian mass[32]. Since our Core model is delocalized among four thermogenic organs and makes no geometric assumptions, we expected higher rates of thermogenesis (rMR/M^c) and lower allometric exponents ("c") in smaller mammals with higher ratios of surface area/volume. Consistent with this expectation, the optimal scalings for the models developed in Carnivora, Primates and Glires were $M^{0.60}$, $M^{0.53}$ and $M^{0.40}$, respectively (Figure 7).

The values of the model parameters in Glires present a striking contrast to those in the carnivore and primate models: a reversal in sign of the coefficient for brain *cMR* in Glires, and a reversal of the relative magnitudes of the coefficients for liver and brain (Figure 7A). These appear to reflect adaptation to the severe size reduction in Glires to 1/80 of the median, or 1/20 of the average body mass of primates (Supplementary Table S3). A complementary reversal was found for the relative magnitudes of VIP, which reflect the degree of model dependence on each organ, rather than the outcome of historical variation (Figure 7B). The elevated VIP value for the brain in primates indicates its significant role in determining the overall rate of Core thermogenesis.

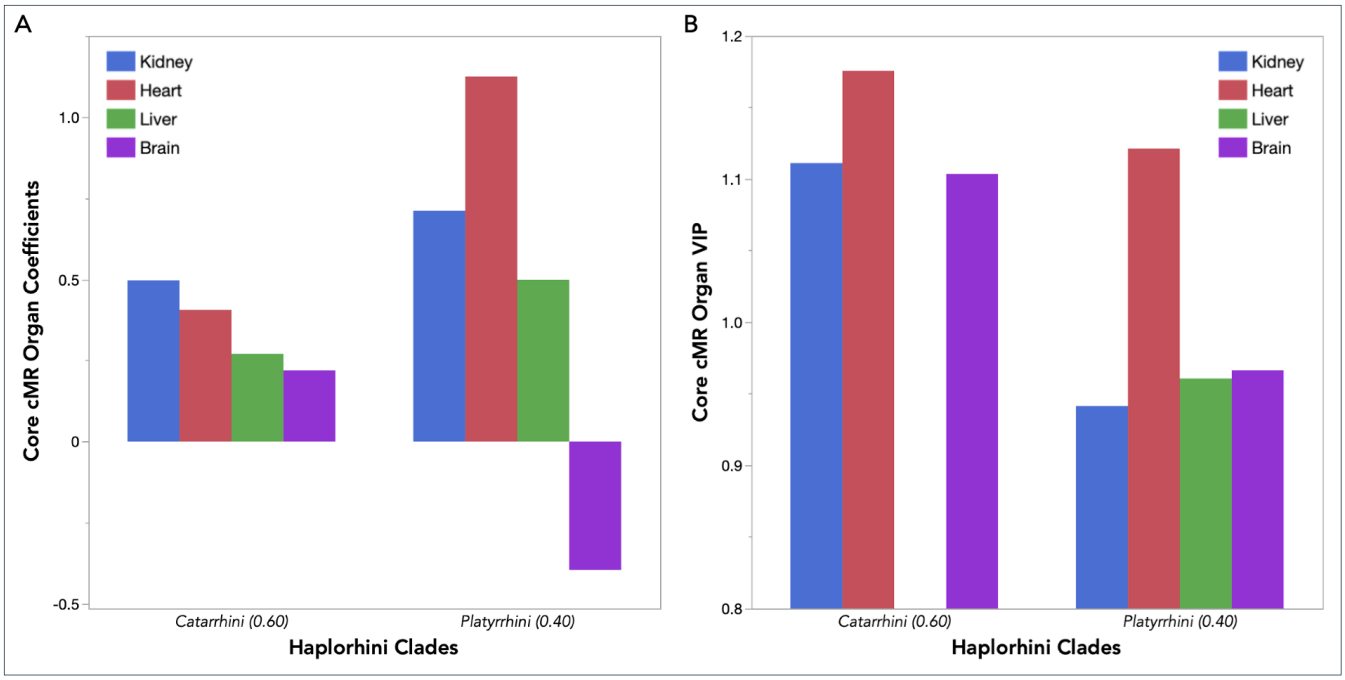

Figure 8. Organ cMR coefficients and VIP values for Core models in Haplorhini.
Values in parentheses next to each clade indicate the optimal allometric exponent of the Core *cMR* model.
A. Organ coefficients for the optimal model Catarrhini (N = 10) and Platyrrhini (N = 8).
B. Organ VIP values above threshold of significance (0.80) for each model (liver VIP = 0.4070).

The same trends were recapitulated and magnified with the divergence of Catarrhini from Platyrrhini. The optimal Core *cMR* allometric exponents diverged from 0.53 among all primates (Figure 7) to 0.60 for the larger Catarrhini and 0.40 for the smaller Platyrrhini (Figure 8). The Platyrrhini model exibited elevated values for both heart coefficient and VIP while among Catarrhini, the VIP for liver dropped to 0.4070, below the 0.8 threshold for significance, indicating a negligible contribution to overall Core thermogenesis (Figure 8) (Supplementary Table S3).

The evolution of organ cMR tradeoffs validates the Core model of thermoregulation

With the preceding evidence that body temperature homeostasis has fine-tuned the sizes of the four Core organs and their rates of thermogenesis, we investigated the historical timing of the resulting tradeoffs. In agreement with the differences predicted by Core *cMR* models (Figures 7 and 8), Bayesian inference revealed opposing directions of evolution between *cMR.80lvr* and body size, both between Haplorhini and Glires, as well as within each clade (Figure 9).

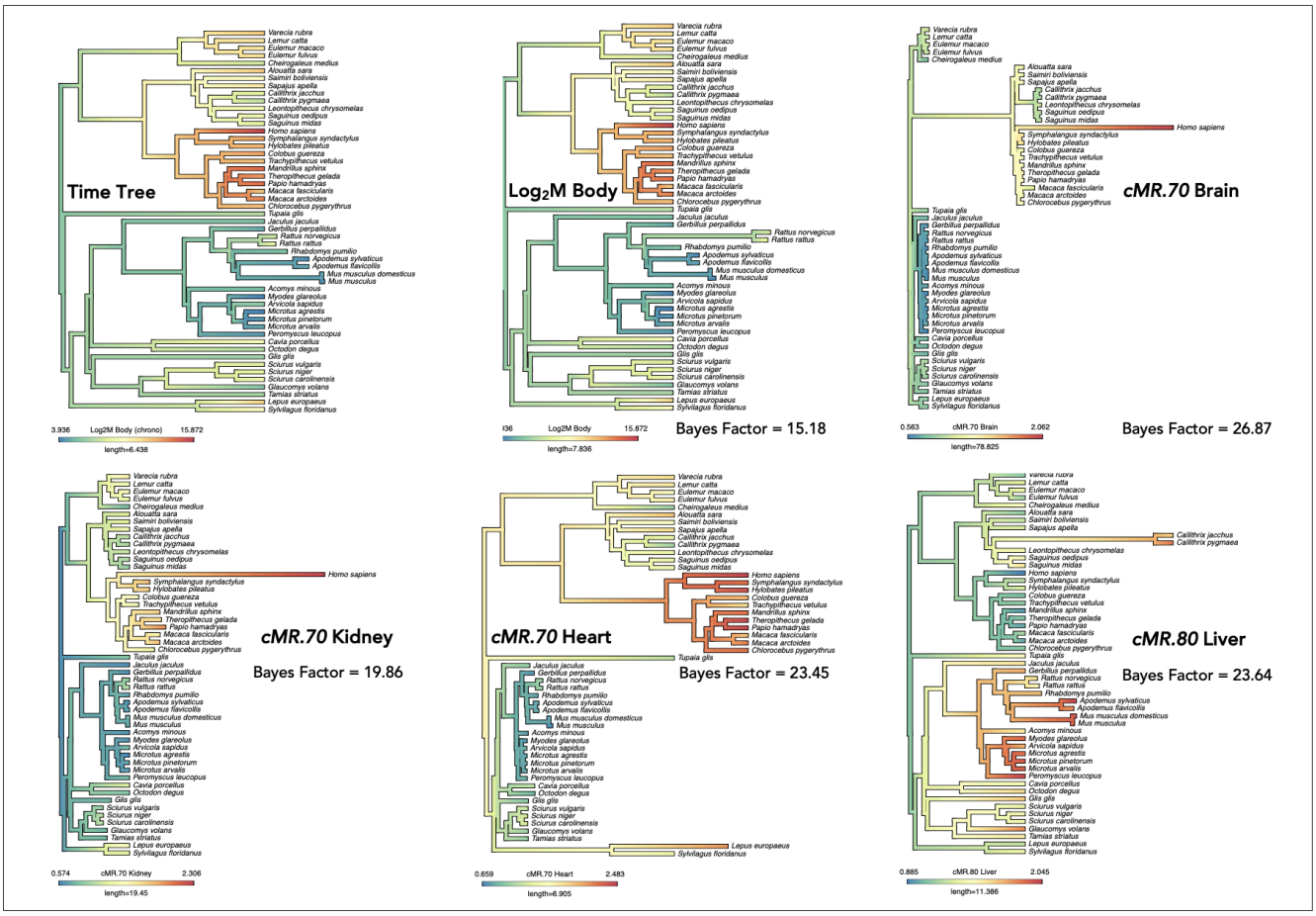

Figure 9. Variable rate phenograms of *Log$_2$M*, *cMR.80lvr*, and *cMR.70* of kidney, heart and brain.
Note that the ancestral values for body size have also been applied to the reference ultrametric tree.
Bayes factors were computed from the difference between the median log likelihood (*Lh*) of the 1% most likely trees and the median *Lh* of the 1% of trees with the smallest non-zero sum of changes to branch length, *i.e.* those trees most similar to the reference time tree[11].

Among primates, an accelerated increase in liver *cMR* accompanied the decrease in size of two of the smallest Platyrrhini, one of which (*Callithrix pygmaea*) may be heterothermic[44]. All five of the smaller (< 1.0 kg) Platyrrhini exhibited elevated levels of *cMR.80lvr*, consistent with adaptation to a low energy regime and increased reliance on gluconeogenesis. Among all Glires, those species that underwent the most severe reduction in size exhibited the greatest increases in liver *cMR.80*; conversely, the largest species (Lagomorphs) exhibited the lowest liver *cMR*s (Figure 9).

Brain *cMR.70* increased in intensity and its rate of evolution accelerated with the divergence of Haplorhini, and again with that of humans, in contrast to its relative stasis in Lemuriformes and Glires (Figure 9). Compared with their ancestors, Glires and the five smallest Platyrrhini exhibited an accelerated *reduction* in brain *cMR.70*, a clade-wide tradeoff that mirrored the size-related tradeoff in Glires between brain and liver *cMR*s. The relative levels of heart *cMR.70* generally tracked body size, with accelerated rates of heart evolution in the clades of the largest Glires (Lagomorpha) and primates (Catarrhini). The divergence of humans was accompanied by an exceptional increase in the rate of evolution of kidney *cMR.70*, as well as that of *cMR.70brn* (Figure 9).

DISCUSSION

Inferring cellular metabolic rates

The recent publication of hundreds of primate genome sequences[45] has been accompanied by ever more fine-grained analyses of the phylogenetic covariance of non-logarithmic traits that may have fueled the evolutionary expansion of brain size in the hominid lineage[46]: diets richer in calories and protein[47-48], more efficient food acquisition and assimilation[49], greater adipose tissue reserves[23,50], and gains in the reliability of gestation, lactation and infant care[51-52]. However, the disposition of the internal heat generated by larger brains has yet to be addressed: while the *bMR* of humans is 50% higher than that of similar-sized orangutans[11], primate whole-body *bMR*s can account for only 35% of relative brain size[53] (37% based on the 24 primates in the present dataset).

The conventional power law model allows the *rMR*s of species varying in mass over several orders of magnitude to be made a linear function of *M* by log transformation, regardless of phylogenetic order[39]. Phylogenetic comparative methods can then be applied to deconvolve adaptive from inherited variation[35-38]. However, the physical and ecological forces to which organ and body *rMR*s have adapted, notably temperature and the availability of water, scale arithmetically. Unlike the fixed *sMR* distribution derived from the slope of log *rMRorg*/log*Morg*, a *cMR* distribution can be matched to the

distribution of a relevant physiological or thermodynamic variable without log transformation, while differences between phylogenetic orders can be resolved by standardization of the ranges of predictor and response variables (see, for example, Supplementary Figures S4 and S9-A).

Thermoregulatory* versus *body size constraints on organ size

Since the seminal analysis by Lande (1979)[31], it has been the convention to base the allometry of brain size on whole body mass[23,54-55]. This approach has not detected significant anticorrelations among organ sizes[23], which is not surprising, given that the mass of each organ is developmentally programmed to track body mass[56]. We have previously shown in mammals that a model of stabilizing selection accounted better for the dependence on *mirFam* of whole-body *cMR* than did a Brownian motion process[11]. The optimal *cMR* scaling in this model of stabilizing selection was $M^{0.75}$ which, in the present study, is uniquely equivalent to the log-based *sMR* of the Core and therefore the zone of minimal constraint on the rate of Core thermogenesis by body size *i.e.* opposite to the whole-body relationship between log *rMR* and log $M^{0.75}$. Moreover, the models of *cMR.75cor* and *sMR.75cor* were dependent only on the *cMR* of the liver. These observations imply a degree of uncoupling of the size of thermogenic organs from body size and suggest a hierarchy of organ size regulation: between clades, organ sizes have been developmentally programmed to track body size while within clades, the relative proportions of the Core organs have been adjusted in response to thermoregulatory demands.

In comparing relative brain size between primates and Glires, Lande (1979) attributed the expansion of brain size in primates to a genetic uncoupling of its dependence on body size[31]. Our thermodynamic models of Core *cMR* in carnivores, primates and Glires, together with Bayesian reconstruction of the evolution of body size, suggest an inversion of Lande's premise, namely that the uncoupling reflects the disproportionate reduction of Glires body size relative to brain size; as a result, the median or average *Mbrn*/*Mbody* ratio found in Glires (N = 26) has actually remained higher than that found in primates (N = 22) ≅ carnivores (N = 30), which is the inverse of the ranking of relative brain size defined as log Mbrn/log Mbdy (Supplementary Table S3) (see also Smaers et al, 2021)[55].

The developmental and phylogenetic plasticity of the liver

Of the six possible *cMR* tradeoffs among four thermogenic organs, the brain - liver tradeoff is the most significant and most highly conserved. Since we detected the brain - liver tradeoff among all the clades of Theria that we examined, and so this plasticity appears to belong to the mammalian evolutionary toolkit. Upon depletion of glycogen in the fasting state, the liver serves as the primary

organ of gluconeogenesis: the glucagon-dependent reduction of amino acid or glycerol carbons, fueled by free fatty acids released from adipose tissue. Gluconeogenesis contributes 40 - 60% of total glucose production after an overnight fast in humans, and greater than 90% after 48 hours of fasting[57]. Liver oxidation of fatty acids also generates ketone bodies that provide 60% of the human brain's energy during a prolonged fast, thereby sparing muscle protein[58]. Elevated levels of circulating fatty acids induce insulin resistance in liver and skeletal muscle[58], an additional mechanism to ensure an uninterrupted supply of glucose to the brain which, unlike these organs, cannot switch to fatty acid oxidation. Interestingly, many of the effectors mediating the transition between the fed state/lipogenesis and the fasting state/lipolysis are also regulated by specific microRNAs[59-61].

Brain glucose utilization peaks around age five in humans, early in the extended period between weaning and sexual maturity, which is also the period of slowest growth in body mass[62]. Based on the turnover of isotopically-labeled glucose, glucose production was proportional to brain mass over the entire lifespan, and therefore highest among young children[63]. Among prepubertal children (7 - 9 years of age), the rate of gluconeogenesis was still 50% higher than that found among adolescents[64-65]. The inverse relationship between developmental changes in the brain's glucose uptake and the rate of body mass growth[62] implicate the liver as the pivotal partner in this ontogenetic tradeoff.

Drawing on metabolite fluxes measured in humans, a computational model of the equivalent fluxes in mice found that following an overnight fast, the rates of liver gluconeogenesis, lipolysis and proteolysis were all elevated ~ 10-fold in mice, relative to the rates in humans[66]. These findings comport well with the opposite directions of evolution of *cMR.80lvr* that we found between Glires and primates, which are associated with divergent body size and life history strategies, notably population turnover[67-69]. The apparent evolutionary plasticity of the liver appears to have co-opted the liver's inherent mechanism of developmental plasticity: among mammalian organs, only the liver retains full regenerative potential[56]. If the evolution of liver size has been constrained both by thermoregulatory demands and the need for glucose production, then a situation of high energy reliability/low dependence on gluconeogenesis in an incipient clade may have permitted a reduction in relative liver size, such as that associated with the divergence of Catarrhini. Conversely, smaller bodies and a tradeoff favoring the liver appear to signify adaptation to limited resources relative to population size, as exemplified by the divergence of Glires from Euarchontoglires, Strepsirrhini from primates, and Platyrrhini from Haplorhini.

Hippo-YAP, the bilaterian regulator of organ size[70], coordinates liver growth with the suppression of gluconeogenesis[71-74]. Significantly, the global underexpression of microRNAs that is frequently observed in tumor cells has been attributed to aberrant density-dependent regulation of the same Hippo-YAP signaling[75]: at low cell densities, Hippo signaling is normally suppressed, allowing YAP to localize in the nucleus and stimulate cellular proliferation, while at normal organ size and tissue density, YAP translocation and activity are inhibited by Hippo[70]. Constitutively active YAP inhibits microRNA biogenesis and causes widespread miRNA suppression in cells and tumors, together with posttranscriptional induction of oncogenic MYC protein[75-76]. Significantly alterating the rate of microRNA biogenesis is expected to cause dysregulation of gene regulatory networks (GRNs), either disrupting the timing of transient signals, such as transcription factors[77-78], or shifting the repression profile of targets regulated by multiple microRNAs[79]. By extension, the evolutionary plasticity of the liver implies shifting setpoints for liver size and activity with respect to body size and temperature; these, in turn, depend on the dynamic ranges for the interactions among Hippo-YAP signaling, organ size, and microRNA biogenesis.

A feedback model for brain size and energy reliability

Assuming that the inverse relationship between the rate of liver thermogenesis and *mirFam* signifies decreasing dependence on gluconeogenesis, we modeled a simple feedback loop: energy reliability facilitates an increase in brain size which, in turn, facilitates improved energy reliability up to the limits imposed by anatomy and physiology, such as the diameter of the birth canal, or the physiological limit on the rate of heat dissipation[8]. Based on the adaptive shifts in *mirFam* coinciding with the emergence of homeothermy and divergence of Catarrhini, we assigned *mirFam* to serve as a proxy for energy reliability. Using a logistic function, we fit *mirFam* to the primate brain size dataset of Grabowski et al (2023)[43]:

$$\frac{d\,(mirFam)}{d\,(\log M_{brn}/\log M_{bdy})} = r \bullet mirFam\,(1 - mirFam/mirFam_{max}),$$

where ***r*** is the growth rate, and the range of *mirFam* has been scaled to a range of 1.0.

As shown in Figure 10A, log *Mbrn*/log *Mbdy* is a predictor of *mirFam,* rather than the converse, lending credence to the proposition that evolutionary increases in brain size were associated with greater energy reliability. Since *mirFam* can also be fit to the relative sizes of the other thermogenic organs (Supplementary Figure S8), the question arose as to which relationship might be the principal target of selection. However, the ranges of *mirFam* are highly clade-specific (Supplementary Figure S9-A), and therefore its variation relative to any trait is always secondary to phylogenetic distance.

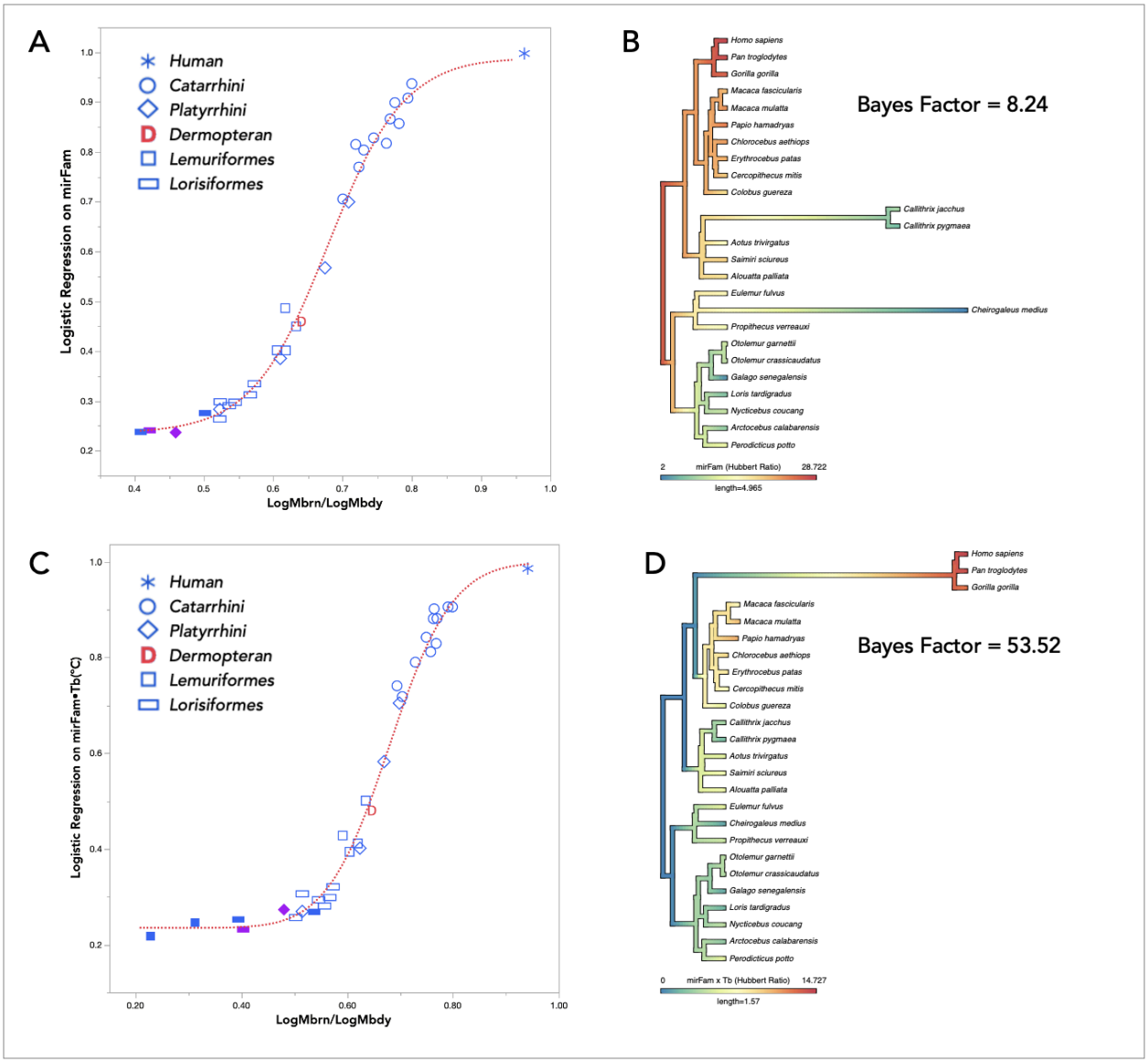

Figure 10. Logistic models of brain size evolution (data from Grabowski et al, 2023)[46].
A, C. For these idealized models, *mirFam* and *mirFam•*T_b (°C) values were those predicted by the original logistic regression models, which excluded the small heterotherm *Cheirogaleus medius*:
R^2 = 1.00 (jitter applied) *versus* the original R^2 = 0.88 and 0.85, respectively.
By comparison, logistic regression of Log *Mbdy* on the ratio Log *Mbrn*/Log *Mbdy* yielded R^2 = 0.83.
B, D. Variable rate phenograms of the Hubbert linearization of the corresponding logistic functions.
D = *Galeopterus variegatus*. Filled symbols: heterotherms (blue), suspected heterotherms (purple).

Having previously demonstrated in mammals that the relationship between whole body *cMR* and *mirFam* has evolved independent of phylogeny[11], we instead compared the dependence of individual organ *cMR*s on *mirFam*. In phylogenetic regressions on *mirFam* of organ *cMR*s ranging from *cMR*.60 - *cMR*.80, all kidney and heart *cMR*s, and all but one liver *cMR* (*cMR.60lvr*), varied independently of phylogenetic distance (Pagel's *lambda* = 0.0) (Supplementary Table S4). In contrast, brain *cMR* variation with respect to *mirFam* was, in every case, secondary to phylogenetic distance (*lambda* =

1.0); thus, divergence of primate clades coincided with changes in the dynamic range of *mirFam* with respect to the determinants of the rate of brain energy expenditure (Supplementary Table S4).

Variable rate phenograms corresponding to this logistic model were generated using the ratios from the Hubbert linearizations of the logistic functions (Figure 10B)[77]. Here the color scale represents rank order, which generally tracks body size. The three smallest species, a Lemuriform and two species of marmoset (*Callithrix*), exhibited an accelerated descent in rank: *Cheirogaleus medius* is a heterotherm, *Callithrix pygmaea* may also be heterothermic[44]. This observation aligns with that previously reported for Callitrichines[55], indicating that the baseline of this logistic function represents a regime of minimal energy reliability, perhaps related to low calorie-density folivory or insectivory[81], a scenario that may also inform the adaptive increase of liver *cMR.80* in the *Callithrix* clade.

Extending this logic, we postulated that the upper plateau of the logistic model, occupied by primates with the largest bodies and relative brain sizes, corresponds to a physiological limit on the rate of heat dissipation[8]. During exercise, human brain temperature increases in parallel with that of the body core, leading to hyperthermia and fatigue[16-18, 82]. Cooling of the brain, the only organ with its own exoskeleton, has been proposed as a benefit of the so-called "oxygen paradox" of neurovascular coupling *i.e.* the surplus blood flow in excess of oxygen demand, elicited by neuronal activation[83-85].

We find that, after correction for phylogeny, body temperatures (T_b) in primates are inversely correlated with *mirFam*, indicating that the product *mirFam* x T_b is evolutionarily conserved. (Supplementary Figure S9-B). Since the highest *mirFam* are found in the largest primates (*Catarrhini*), this is reminiscent of the opposite trends, on a broad mammalian scale, between body size[1] and body temperature[2]. When Boreoeutheria were ordered by overall metabolic rate (*cMR.75bdy*), the values of *mirFam* x T_b oscillated around the values of log C_{min}, further indication that the product *mirFam* x T_b tracks the physiological limit on the rate of heat dissipation limit (Supplementary Figure S10). Thus, the accelerated evolution detected among hominid apes near the plateau of a *mirFam* x T_b logistic model (Figure 9D) is consistent with adaptation to this limit[8].

In keeping with the long-range evolutionary patterns for mammalian body size[1] and temperature[2], Bayesian inference predicted opposite trends for *mirFam* and *mirFam* x T_b with respect to relative brain size: descending in rank on the *mirFam* tree, except among Catarrhini, and ascending in rank on the tree for *mirFam x* T_b (Figure 10C and D, respectively). Thus, our logistic model assigns the ancestral

primate a high rank for energy reliability and a low rank relative to the heat dissipation limit, a propitious combination for the founder of a new order of mammals on a new fitness landscape[86]. In many respects this model, derived from the reparametrization of organ rates of energy consumption in terms of *mirFam*-based *cMR*s, fulfills the recent call for an explanation of the distinct pattern of brain size evolution in primates "in terms of the release of a constraint or an adaptive shift that initiated escalating feedback between brain and behavior"[10]. Together with the Core model of thermoregulation[32], it has allowed us to uncover a conserved energy tradeoff that was first proposed 40 years ago in order to account for the expansion of brain size in the human lineage[21]. Since this logistic model is agnostic regarding underlying mechanisms, it may also serve as a null hypothesis for comparison with the evolution of candidate mechanisms of adaptation.

Implications for evolutionary medicine

The reparametrization of *cMR*s also has far-reaching implications for evolutionary medicine[87]. For example, human kidney *cMR.70* underwent an adaptive increase to a level 30% higher than found in other hominoid apes; by comparison, the value for the human was 10% *lower* when scaled according to the slope (0.90) of log *rMRkdn*/log *Mkdn*. Since the kidney is responsible for the homeostasis of pH, nitrogen, sodium, water and glucose, the rapid evolution *cMR.70kdn* in humans may represent adaptation to a diet enriched in lipid and protein[47-48], or to an altered landscape of opportunities for hydration *versus* risks of dehydration ("Savanna hypothesis")[27-30]. A related adaptation, a high density of eccrine sweat glands[25], may have enabled early humans to run down game in long distance pursuits[88], but may also have made them uniquely susceptible to dehydration[26], a marathon-enabling tradeoff. As it is, the kidneys of modern humans are quite susceptible to damage by heat stress: exposure to 40°C for as little as one hour is sufficient to redirect blood flow to the skin, reduce blood flow to the kidney by one third[89] and trigger responses promoting water conservation that can eventually lead to acute kidney injury, such as activation of the renin-angiotensin-aldosterone system[90-91]. The kidneys of our hominid ancestors may have been even more vulnerable to heat and aridity, prior to this adaptive increase in *cMR.70kdn*.

Simulation of two million years of African and Eurasian climate and habitats supports the view that *H. sapiens* evolved from *H. heidelbergensis* in southern Africa during an unusually warm period that would have necessitated adaptation to hotter, drier conditions[30]. It is not generally appreciated[92] that maintenance of temperature homeostasis and water balance may have driven another uniquely human adaptation, the remarkable ability to store fat. For example, camels and fat-tailed sheep represent two

genera that manifest excess adiposity, relative to non-desert adapted ungulates[93-94]. Together with studies of aboriginal populations inhabiting the same arid regions for thousands of years, evidence of more rapid evolution and differential expression has been found among desert-adapted mammals for genes or gene families mediating lipid metabolism, insulin responsiveness, water and solute transport, as well as the activity of renin-angiotensin-aldosterone complex[95].

Adipose tissue was found to make up 41% of the body mass in adult women, compared to 9% in chimpanzee and 14% in gorilla females[15]. In addition to prolonging the ability to release fatty acids, thereby sparing glucose for the brain, fatty acid oxidation generates a high molar ratio of water, which may appreciably affect overall water balance[96]: rats fed a high fat diet consumed less water following deprivation[97], and men who are obese manifested diminished thirst in response to dehydration[98]. The permanent enlargement of breast tissue, in addition to providing nutrition during the extended infancy of humans, may have served a thermoregulatory function in a savanna environment that was hotter by day and cooler by night[99-100], as well as a portable buffer against infant dehydration. In sum, detection of the adaptive increase in human kidney *cMR* in the ancestors of modern humans leads to a reappraisal of some of the other adaptations associated with the transition to a savanna ecosystem, which may represent overlapping nutritional and thermoregulatory functions.

SYNTHESIS

The adaptive value of repression by individual microRNAs operating in gene regulatory networks (GRNs) has been attributed to their ability to canalize phenotype expression by buffering the effects of environmental or allelic variation[101-102], to set thresholds for cell fate determination, and to maintain the identity of differentiated cells by defining ranges of protein expression[103-105]. Major stages in the diversification of animal cell types, morphologies and complexity of behavior have coincided with significant expansions of microRNA and target repertoires[106-109]. For example, the emergence of placental mammals coincided with the appearance of 13 novel implantation-related microRNA families[110], and the cognitive success of the genus *Octopus* has been linked to 34 novel microRNA families that are preferentially expressed in neural tissues[111]. However, these *post hoc* associations do not shed light on the conditions favoring repertoire expansion, nor how the emergence of new characteristics is related to the total number of families (*mirFam*), as opposed to the individual activities of new microRNAs[105].

The emergence of permanent homeothermy in the ancestral clade of Boreoeutheria and the attendant acceleration of metabolic rates coincided with a 15% expansion of the number of microRNA families[11], consistent with evidence that microRNAs were required to synchronize the activity of developmental GRNs with metabolic rates[77]. A similar *mirFam* expansion accompanied the divergence of Catarrhini: in this study, we have been able to chart *mirFam* as a function of relative brain size, without reference to phylogeny, and link it to a reciprocal decline in thermogenesis by the liver, the primary organ of gluconeogenesis. These observations suggest that a high level of energy reliability, and presumably fitness, in an incipient clade may be a precondition for a significant expansion of the microRNA repertoire. What appear in the evolutionary record as clade-wide shifts to a higher number of microRNA families[112] and higher density of conserved target sites[11] would have necessitated a global reset of the dynamic ranges of microRNAs with respect to effector pathways, and the repression profiles of targets that are regulated by multiple microRNAs[79]. While microRNA levels are stabilized by numerous homeostatic mechanisms[113-120], the robustness of such GRNs may have actually facilitated, rather than impeded, the emergence of new or enhanced phenotypes[121-123]. These two examples of repertoire expansion, the emergence of permanent homeothermy[11] and the expansion of brain size in Catarrhini, together with the observation that losses of microRNA families have occurred much less frequently than gains[121], support the inference of an evolutionary ratchet mechanism, governed by selection for energy reliability, that links the evolution of more complex traits to the expansion of the microRNA repertoire.

DECLARATIONS

Limitations

The three principal limitations of this study are:

i) the indirect origin of the mammalian organ *sMR*s in the main dataset (Supplementary Table S1). These have been inferred based on organ mass from a single set of direct measurements in humans (Elia, 1992)[15], as in the case of all subsequent studies of the evolution of mammalian organ *MR*s.

ii) the small number and variable quality of the body temperature data in the AnAge database[5];

iii) systematic undercounting of the number of conserved microRNA families by the MirMachine algorithm[6], relative to the reference, manually-curated database (currently MirGeneDB 3.0)[7].

These factors are not expected to affect the qualitative interpretation of our results.

Data Availability

All original data with accompanying references are provided in Supplementary Tables S1 - S4.

Acknowledgment

BF is supported by the Tromsø forskningsstiftelse (TFS) [20_SG_BF 'MIRevolution'].

Author Contributions

Conceptualization: TS; Methodology: TS; Investigation: BF and TS; Writing – Original Draft: TS; Writing – Review & Editing: BF and TS; Visualization: TS; Funding Acquisition: BF.

Declaration of Interests

The authors declare no competing interests.

Statement on the use of AI

No part of this work was generated or edited using AI.

REFERENCES

1. Baker J, Meade A, Pagel M and Venditti C. 2015. Adaptive evolution toward larger size in mammals. *Proc Natl Acad Sci USA* **112**: 5093-5098.

2. Avaria-Llautureo J, Hernandez CE, Rodriguez-Serrano E and Venditti, C. 2019. The decoupled nature of basal metabolic rate and body temperature in endotherm evolution. *Nature* **572**: 651-654.

3. Naya DE, Spangenberg L, Naya H and Bozinovic F. 2013. Thermal conductance and basal metabolic rate are part of a coordinated system for heat transfer regulation. *Proc Roy Soc B* **280**: 20131629.

4. Fristoe TS, Burger JR, Balk MA, Khaliq I, Hof C and Brown JH. 2015. Metabolic heat production and thermal conductance are mass-independent adaptations to thermal environment in birds and mammals. *Proc Natl Acad Sci USA* **112**: 15934-15939.

5. Araújo MB, Ferri-Yáñez F, Bozinovic F, Marquet PA, Valladeres F and Chown SL. 2013. Heat freezes niche evolution. *Ecol Letters* **16**: 1206-1219.

6. Khaliq I, Hof C, Prinzinger R, Böhning-Gaese K and Pfenninger M. 2014. Global variation in thermal tolerances and vulnerability of endotherms to climate change. *Proc Roy Soc B* **281**: 20141097.

7. Bennett JM, Sunday J, Calosi P, Villalobos F, Martínez B, Molina-Venegas R, Araújo MB, Algar AC, Clusella-Trulas S, Hawkins BA, Keith SA, Kühn I, Rahbek C, Rodríguez L, Singer A, Morales-Castilla I and Olalla-Tárraga MA. 2021. The evolution of critical thermal limits of life on Earth. *Nature Comm* **12**: 1198.

8. Speakman JR and Król E. 2010. Maximal heat dissipation capacity and hyperthermia risk: neglected key factors in the ecology of endotherms. *J Anim Ecol* **79**: 726-746.

9. Heldstab SA, Isler K, Graber SM, Schuppli C and van Schaik. 2022. The economics of brain size evolution in vertebrates. *Curr Biol* **32**: R697-R708.

10. Venditti, C, Baker J and Barton RA. 2024. Co-evolutionary dynamics of mammalian brain and body size. *Nat Ecol Evol* **8**: 1534–1542.

11. Fromm B and Sorger T. 2023. Rapid adaptation of cellular metabolic rate to the microRNA complements of mammals and its relevance to the evolution of endothermy. *iScience* **27**: 108740.

12. Boyles JG, Thompson AB, McKechnie AE, Malan E, Humphries MM and Careau. 2013. A global heterothermic continuum in mammals. *Global Ecol Biogeogr* **22**: 1029-1039.

13. Ruf T and Geiser F. 2015. Daily torpor and hibernation in birds and mammals. *Biol Rev* **90**: 891-926.

14. Clavel J and Morlon H. 2017. Accelerated body size evolution during cold climatic periods in the Cenozoic. *Proc Natl Acad Sci USA* **114**: 4183-4188.

15. Pontzer H, Brown MH, Raichlen DA . . (many others) . . Ross SR. 2016. Metabolic acceleration and the evolution of human brain size and life history. *Nature* **533**: 390-393.

16. Nybo L. Brain temperature and exercise performance. 2012. *Exp Physiol* **97**: 333-339.

17. Wang H, Wang B, Normoyle K, Jackson K, Spitler K, Sharrock MF, Miller CM, Best C, Llano D and Du R. 2014. Brain temperature and its fundamental properties: a review for clinical neuroscientists. *Front Neurosci* **307**: 1-17.

18. Sung D, Risk BB, Kottke PA, Allen JW, Nahab F, Fedorov AG and Fleischer CC. 2022. Comparisons of healthy human brain temperature predicted from biophysical modeling and measured with whole brain MR thermometry. *Nature Sci Rep* **12**:19285.

19. Lassen NA. 1985. Normal average value of cerebral blood flow in younger adults is 50 ml/100 g/min. *J Cereb Blood Flow Metab* **5**: 347-349.

20. Claassen JAHR, Thijssen DHJ, Panerai RB and Faraci FM. 2021. Regulation of cerebral blood flow in humans: physiology and clinical implications of autoregulation. *Physiol Rev* **101**: 1487-1559.

21. Armstrong E. 1983. Relative brain size and metabolism in mammals. *Science* **220**: 1302-1304.

22. Aiello LC and Wheeler P. 1995. The expensive-tissue hypothesis: the brain and the digestive system in human and primate evolution. *Curr Anthro* **36**: 199-221.

23. Navarette A, van Schaik CP and Isler K. 2011. Energetics and the evolution of human brain size. *Nature* **480**: 91-93.

24. Lindshield S, Hernandez-Aguilar RA, Korstjens AH . . (many others) . . Yoshikawa M. 2021. Chimpanzees (*Pan troglodytes*) in savanna landscapes. *Evol Anthropol* **30**: 399-420.

25. Kamberova YG, Guhana SM, DeMarchisa A, Jianga J, Wright SS, Morgan BA, Sabetid PC, Tabina CJ, and Lieberman DE. 2018. Comparative evidence for the independent evolution of hair and sweat gland traits in primates. *J Hum Evol* **125**: 99–105.

26. Hora M, Pontzer H, Wall-Scheffler CM and Sládek V. 2020. Dehydration and persistence hunting in *Homo erectus*. *J Hum Evol* **138**:102682.

27. Dart, RA. *Australopithecus africanus*: the man–ape of South Africa. 1925. *Nature* **115**: 195-199.

28. Reed KE. Early hominid evolution and ecological change through the African Plio-Pleistocene. 1997. *J Hum Evol* **32**: 289-322.

29. Davies TJ, Daru BH, Bezeng BS . . (many others) . . Bond WJ. 2020. Savanna tree evolutionary ages inform the reconstruction of the paleoenvironment of our hominin ancestors. *Sci Rep* **10**: 12430.

30. Timmermann A, Yun KS, Raia P . . (many others) . . Ganopolski. 2022. Climate effects on archaic human habitats and species succession. *Nature* **604**: 495-501.

31. Lande R. 1979. Quantitative genetic analysis of multivariate evolution applied to the brain: body size allometry. *Evolution* **33**: 402-416.

32. Porter WP and Kearney M. 2009. Size, shape, and thermal niche of endotherms.
Proc Natl Acad Sci USA **106**: 19666-19672.

33. Nettelbeck AR. 1997. Sightings of binturongs in the Khao Yai national park. *Small Carniv Consvn* **16**: 22-24.

34. Grassman LI, Tewes, ME and Silvy NJ. 2005. Ranging, habitat use and activity patterns of binturong *Arctictis binturong* and yellow-throated marten *Martes flavigula* in north-central Thailand. *Wldlf Biol* 11: 49-57.

35. Felsenstein J. 1985. Phylogenies and the comparative method. *Amer Naturalist* **125**: 1-15.

36. Hansen TF. 1997. Stabilizing selection and the comparative analysis of adaptation. *Evolution* **51**: 1341-1351.

37. Pagel M. 1999. Inferring the historical patterns of biological evolution. *Nature* **401**: 877-884.

38. Pagel M, O'Donovan C and Meade A. 2022. General statistical model shows that macro-evolutionary patterns and processes are consistent with Darwinian gradualism. *Nature Comm* **13**: 1113.

39. Kleiber M. Body size and metabolism. 1932. *Hilgardia* **6**: 315-353.

40. Scholander PF, Hock F, Walters V, Johnson F and Irving L. 1950. Heat Regulation in Some Arctic and Tropical Mammals and Birds. *Biol Bull* **99**: 237-258.

41. de Jong S. SIMPLS: 1993. An alternative approach to partial least squares regression.
Chemometrics and Intelligent Laboratory Systems **18**: 251-263.

42. Wold S, Johansson E. and Cocchi, M. 1993. PLS: partial least squares projections to latent structures.
In *Drug Design: Theory, Methods and Applications* (pp. 523-550). Kluwer ESCOM Science Publisher.

43. Celeux G and Govaert G. Gaussian Parsimonious Clustering Models. 1995. *Pattern Recognition* **28**: 781-793.

44. Tattersall GJ. 2012. Diurnal changes in metabolic rate in pygmy marmosets: Implications for sleep, torpor, and basal metabolism in primates. In: Ruf, T., Bieber, C., Arnold, W., Millesi, E. (eds)
Living in a Seasonal World, chapter 41: 471-480. Springer.

45. Kuderna LFK, Gao H, Janiak MC . . (many others) . . Bonet TM. 2023.
A global catalog of whole-genome diversity from 233 primate species. *Science* **380**: 9-913.

46. Grabowski M, Kopperud BT, Tsuboi M and Hansen TF. 2023. Both diet and sociality affect primate brain-size evolution. *Syst Biol* **72**: 404-418.

47. Simmen B, Pasquet P, Masi S, Koppert GJA, Wells JCK and Hladik CM. 2017. Primate energy input and the evolutionary transition to energy-dense diets in humans. *Proc Roy Soc B* **284**: 20170577.

48. Paine OCC, Koppa A, Henry AG . . (many others) . . Sponheimer M. 2019. Seasonal and habitat effects on the nutritional properties of savanna vegetation: Potential implications for early hominin dietary ecology.
J Hum Evol **133**: 99-107.

49. Zeller E, Timmermann A, Yun KY, Raia P, Stein K and Ruan J. 2023. Human adaptation to diverse biomes over the past 3 million years. *Science* **380**: 604 - 608.

50. Mascia-Lees FE, Relethford JH and Sorger T. 1986. Perspectives on permanent breast enlargement in human females. *Amer Anthro* **88**: 423-428.

51. Martin RD. 1996. Scaling of the mammalian brain: the maternal energy hypothesis. *Physiology* **11**: 149-156.

52. Isler K and van Schaik CP. 2012. Allomaternal care, life history and brain size evolution in mammals. *J Human Evol* **63**: 52-63.

53. Isler K, Kirk EC, Miller JMA, Albrecht GA, Gelvin GR and Martin RD. 2008. Endocranial volumes of primate species: scaling analyses using a comprehensive and reliable data set. *J Human Evol* **55**:967-978.

54. Burger JR, George MA, Leadbetter C and Shaikh F. 2019. The allometry of brain size in mammals. *J Mammal* **100**: 276-283.

55. Smaers JB, Rothman RS, Hudson DR . . (many others) . . Safi K. 2021. The evolution of mammalian brain size. *Sci Adv* **7**: eabe2101.

56. Penzo-Méndez AI and Stanger BZ. 2015. Organ-size regulation in mammals. *Cold Spring Harb Perspect Biol* **7**: a019240.

57. Chung ST, Chacko SK, Sunehag AL and Haymond MW. 2015. Measurements of gluconeogenesis and glycogenolysis: a methodological review. *Diabetes* **64**: 3996-4010.

58. Palmer BF and Clegg DJ. 2021. Starvation ketosis and the kidney. *J Nephrol* **52**: 467-478.

59. Ramírez CM, Goedeke L, Rotllan N, Yoon JH, Cirera-Salinas D, Mattison JA, Suárez Y, de Cabo R, Gorospe M and Fernández-Hernando C. 2013. MicroRNA 33 regulates glucose metabolism. *Mol Cell Biol* **33**: 2891–2902.

60. Agbu P and Carthew RW. 2021. MicroRNA-mediated regulation of glucose and lipid metabolism. *Nature Rev Mol Cell Biol* 22: 425-438.

61. Price NL, Goedeke L, Suárez Y and Fernández-Hernando C. 2021. miR-33 in cardiometabolic diseases: lessons learned from novel animal models and approaches. *EMBO Mol Med* 13:e12606.

62. Kuzawa CW, Chugani HT, Grossman LI, Lipovich L, Muzik O, Hof PR, Wildman DE, Sherwood CC, Leonard WR and Lange N. 2021. Metabolic costs and evolutionary implications of human brain development. *Proc Natl Acad Sci USA* **111**: 13010-13015.

63. Bier DM, Leake RD, Haymond MW, Arnold KJ, Gruenke LD, Sperling MA and Kipnis DM. 1977. Measurement of "true" glucose production rates in infancy and childhood with 6,6-Dideuteroglucose. *Diabetes* **25**: 1016-23.

64. Sunehag AL, Treuth MS, Toffolo G, Butte NF, Cobelli C, Bier DM and Haymond MW. 2001. Glucose production, gluconeogenesis, and insulin sensitivity in children and adolescents: an evaluation of their reproducibility. *Ped Res* **50**: 115-123.

65. Sunehag AL, Toffolo G. Treuth MS, Butte NF, Cobelli C, Bier DM and Haymond MW. 2002. Effects of dietary macronutrient content on glucose metabolism in children. *J Clin Endocrin Metab* **87**: 5168-5178.

66. Kummitha CM, Kalhan SC, Saidel GM and Lai N. 2014. Relating tissue/organ energy expenditure to metabolic fluxes in mouse and human: experimental data integrated with mathematical modeling. *Physiol Rep* **2**: e12159.

67. Jeschke JM, Gabriel W and Kokko H. 2008. r-Strategist/K-Strategists. Jørgensen SE and Fath BD, eds. *Encyclopedia of Ecology*: 3113-3122.

68. Dańko MJ, BurgerO, Argasiński K and Kozłowski J. 2018. Extrinsic mortality can shape life-history traits, including senescence. *Evol Biol* **45**: 395-404.

69. de Vries C, Galipaud M and Kokko H. 2023. Extrinsic mortality and senescence: a guide for the perplexed. *Peer Community Journal* **3**: e29.

70. Camargo FD, Gokhale S, Johnnidis JB, Fu D,1 Bell GW, Jaenisch R, and Brummelkamp TR. 2007. YAP1 increases organ size and expands undifferentiated progenitor cells. *Curr Biol* **17**: 2054-2060.

71. Hu Y Shin DJ, Pan H, Lin Z, Dreyfuss JM, Camargo FD, Miao J, and Biddinger SB. 2017. YAP suppresses gluconeogenic gene expression via PGC1α. *Hepatol* **66**: 2029–2041.

72. Cox AG, Tsomides A, Yimlamai D . . . Goessling W. 2018. Yap regulates glucose utilization and sustains nucleotide synthesis to enable organ growth. *EMBO J* **37**: e100294.

73. Ibar C and Irvine KD. 2020. Integration of Hippo-Yap signaling with metabolism. *Dev Cell* **54**: 256-267.

74. Driskill JH and Pan D. 2021. The Hippo pathway in liver homeostasis and pathophysiology. *Ann Rev Pathol Mech Dis* **16**: 299-322.

75. Mori M, Triboulet R, Mohseni M, Schlegelmilch K, Shrestha K, Camargo FD and Gregory RI. 2014. Hippo signaling regulates Microprocessor and links cell-density-dependent miRNA biogenesis to cancer. *Cell* **156**: 893–906.

76. Zhao B, Wei X, Li W . . . Guan KL. 2007. Inactivation of YAP oncoprotein by the Hippo pathway is involved in cell contact inhibition and tissue growth control. *Genes Dev* **21**: 2747-2761.

77. Cassidy JJ, Bernasek SM, Bakker R, Giri R, Peláez N, Bobrowska A, Bagheri N, Nunes Amaral LA and Carthew RW. 2019. Repressive gene regulation synchronizes development with cellular metabolism. *Cell* **178**: 980-992.

78. Keuls RA, Oh YS, Patel I and Parchem RJ. 2023. Post-transcriptional regulation in cranial neural crest cells expands developmental potential. *Proc Natl Acad Sci USA* **120**: e2212578120.

79. Schmiedel JM, Klemm SL, Zheng Y, Sahay A, Blüthgen N, Marks DS and van Oudenaarden A. 2015. MicroRNA control of protein expression noise. *Science* **348**: 128-132.

80. Hubbert MK. 1982. Techniques of prediction as applied to the production of oil and gas. In Gass, Saul I. (ed.) *Oil and Gas Supply Modeling* (proceedings of a symposium held at the Department of Commerce, Washington, DC, June 18–20, 1980). National Bureau of Standards Special Publication **631**: 16-141. Washington (DC).

81. Schiel N and Souto A. 2017. The Common Marmoset: an overview of its natural history, ecology and behavior. *Dev Neurobiol* **77**: 244–262.

82. Tsuji B, Hayashi K, Kondo N and Nishiyasu T. 2016. Characteristics of hyperthermia-induced hyperventilation in humans. *Temperature* **3**: 146-160.

83. Yablonskiy DA, Ackerman JJH and Raichle MR. 2000. Coupling between changes in human brain temperature and oxidative metabolism during prolonged visual stimulation.
Proc Natl Acad Sci USA **97**: 7603-7608.

84. Leithner C and Royl G. 2014. The oxygen paradox of neurovascular coupling.
J Cereb Blood Flow Metab **34**: 19-29.

85. Drew PJ. 2022. Neurovascular coupling: motive unknown. *Trends Neurosci* **45**: 809-819.

86. Erwin DH. 2015. Novelty and innovation in the history of life. *Current Biol* **25**: R930-R940.

87. Benton ML, Abraham A, LaBella AL, Abbot P, Rokas A, Capra JA. 2021.
The influence of evolutionary history on human health and disease. *Nat Rev Genet* **22**: 269-283.

88. Morin E and Winterhalder B. 2024. Ethnography and ethnohistory support the efficiency of hunting through endurance running in humans. *Nature Hum Behav* **8**: 1065-1075.

89. Rowell LB. 1974. Human cardiovascular adjustments exercise and thermal stress. *Physiol Rev* **54**: 75-159.

90. Chapman CL, Johnson BD, Vargas NT, Hostler D, Parker MD, Schlader ZJ. 2020. Both hyperthermia and dehydration during physical work in the heat contribute to the risk of acute kidney injury.
J Appl Physiol **128**: 715–728.

91. Chapman CL, Johnson BD, Parker MD, Hostler D, Pryor RR and Schlader Z. 2021. Kidney physiology and pathophysiology during heat stress and the modification by exercise dehydration, heat acclimation and aging. *Temperature* **8**: 108-159.

92. Heldstab SA, van Schaik CP and Isler I. 2016. Being fat and smart:
A comparative analysis of the fat-brain trade-off in mammals. *J Human Evol* **100**: 25-34.

93. Wu H, Guang X, Al-Fageeh MB, Cao J, Pan S, Zhou H, Zhang L, Abutarboush MH . . (many others) . .
Wang J. 2014. Camelid genomes reveal evolution and adaptation to desert environments. *Nature Comm* **5**: 5188.

94. Xu YX, Wang B, Jing JN, M R, Luo YH, Li X, Yan Z, Liu YJ, Gao L, Ren YL, Li MH and Lv FH. 2023. Whole-body adipose tissue multi-omic analyses reveal molecular mechanisms underlying local adaptation to extreme environments. *Comm Biol* **6**: 159.

95. Rocha JL, Godinho R, Brito JC and Nielsen R. 2021. Life in deserts: the genetic basis of mammalian desert adaptation. *Trends Ecol Evol* **36**: 637-650.

96. Donald J and Pannabecker TL. 2015. Osmoregulation in Desert-Adapted Mammals. In: Hyndman, K, Pannabecker T. (eds) *Sodium and Water Homeostasis*. Physiology in Health and Disease. Springer, New York.

97. Dos-Santos RC, Ishioka G, Cognuck SQ, Mantovani M, Caliman IF, Elias LLK and Antunes-Rodrigues J. 2022. High-fat diet changes the behavioural and hormonal responses to water deprivation in male Wistar rats. *Exp Physiol* **107**: 1454-1466.

98. Chang DC, Stinson EJ, Piaggi P, Krakoff J and Gluck MR. 2023. Disinhibition augments thirst perception from two dehydrating stimuli in men. *Appetite* **182**: 106429.

99. Pawłowski B. 1999. Permanent breasts as a side effect of subcutaneous fat tissue increase in human evolution. *Homo J Comp Hum Biol* **50**: 149–162.

100. Pawłowski B and Zełazniewicz. 2021. The evolution of perennially enlarged breasts in women: a critical review and a novel hypothesis. *Biol Rev* **96**: 2794-2809.

101. Hornstein H and Shomron N. 2006. Canalization of development by microRNAs. *Nature Genetics* **38**: S20-S24.

102. Li X, Cassidy JJ, Reinke CA, Fischboeck S and Carthew RW. 2009. A microRNA imparts robustness against environmental fluctuation during development. *Cell* **137**: 273-282.

103. Mukherji S, Ebert MS, Zheng GXY, Tsang JS, Sharp PA and van Oudenaarden A. 2011. MicroRNAs can generate thresholds in target gene expression. *Nature Genetics* **43**: 854-859.

104. Ebert MS and Sharp PA. 2012. Roles for MicroRNAs in conferring robustness to biological processes. *Cell* **149**: 515-524.

105. Zolboot N, Du JX, Zampa F and Lippi G. 2021. MicroRNAs instruct and maintain cell type diversity in the nervous system. *Front Mol Neurosci* **14**: 646072.

106. Makeyev EV and Maniatis T. 2008. Multilevel Regulation of Gene Expression by MicroRNAs. *Science* **319**: 1789-1790.

107. Erwin DH, Laflamme M, Tweedt SM, Sperling EA, Pisani D and Peterson KJ. 2011. The Cambrian conundrum: early divergence and later ecological success in the early history of animals. *Science* **334**: 1091-1097.

108. Dexheimer PJ and Cochella L. 2020. MicroRNAs: from mechanism to organism. *Front Cell Dev Biol* **8**: 409.

109. Peterson KJ, Beavan A, Chabot PJ, McPeek MA, Pisani D, Fromm B and Simakov O. 2022. MicroRNAs as Indicators into the Causes and Consequences of Whole-Genome Duplication Events. *Mol Biol Evol* **39**: msab344.

110. Taylor AS, Tinning H, Ovchinnikov V, Edge J, Smith W, Pullinger AL, Sutton RA, Constantinides B, Wang D, Forbes K, Forde N and O'Connell MJ. 2023. A burst of genomic innovation at the origin of placental mammals mediated embryo implantation. *Comm Biol* **6**:459.

111. Zolotarov G, Fromm B, Legnini I, Ayoub S, Polese G, Maselli V, Chabot PJ, Vinther J, Styfhals S, Seuntjens E, Di Cosmo A, Peterson KJ and Rajewsky N. 2022. MicroRNAs are deeply linked to the emergence of the complex octopus brain. *Sci Adv* **8**: eadd9938.

112. Fromm B, Høye E, Domanska D, Zhong X, Aparicio-Puerta E, Ovchinnikov V, Umu SU, Chabot, PJ, Kang W, Aslanzadeh M, Tarbier M, Mármol-Sánchez E, Urgese G, Johansen M, Hovig E, Hackenberg M, Friedländer MR and Peterson KJ. 2021. MirGeneDB 2.1: toward a complete sampling of all major animal phyla. *Nucl Acids Res* **50**: D204-D210.

113. Smibert P, Bejarano F, Wang D, Garaulet DL, Yang J, Martin R, Bortolamiol-Becet D, Robine N, Hiesinger PR, and Lai EC. 2011. A *Drosophila* genetic screen yields allelic series of core microRNA biogenesis factors and reveals post-developmental roles for microRNAs. *RNA* **17**: 1997-2010.

114. Ghini F, Rubolino C, Climent M, Simeone I, Marzi MJ and Nicassio F. 2018. Endogenous transcripts control miRNA levels and activity in mammalian cells by target-directed miRNA degradation. *Nat Commun* **9**: 3119.

115. Gebert LFR and MacRae IJ. 2019. Regulation of microRNA function in animals. *Nature Rev Mol Cell Biol* **20**: 21-37.

116. Sheu-Gruttadauria J, Pawlica P, Klum SM, Wang, S, Yario TA, Schirle Oakdale NT, Steitz JA and MacRae IJ. 2019. Structural Basis for Target-Directed MicroRNA Degradation. *Mol Cell* **75**, 1243–1255.

117. Cui Y, Lu X, Ding L, Ke L, Yang D, Pirouz M, Qi Y, Ong J, Gao G, Du P and Gregory RI. 2021. Global miRNA dosage control of embryonic germ layer specification. *Nature* **593**: 602-606.

118. Kingston ER, Blodgett LW and Bartel DP. 2022. Endogenous transcripts direct microRNA degradation in Drosophila, and this targeted degradation is required for proper embryonic development. *Mol Cell* **82**: 3872–3884.

119. Komatsu S, Kita H and Suzuki HI. 2023. Network regulation of microRNA biogenesis and target interaction. *Cells* **12**: 306.

120. Hiers NM, Li T, Traugot CM and Xie M. 2024. Target-directed microRNA degradation: Mechanisms, significance, and functional implications. *Wiley Interdiscip Rev RNA* **15**: e1832.

121. Ciliberti S, Martin OC and Wagner A. 2007. Innovation and robustness in complex regulatory gene networks. *Proc Natl Acad Sci* USA **104**: 13591-13596.

122. Barve A and Wagner A. 2013. A latent capacity for evolutionary innovation through exaptation in metabolic systems. *Nature* **500**: 203-206.

123. Catalán P, Wagner A, Manrubia S and Cuesta JA. 2018. Adding levels of complexity enhances robustness and evolvability in a multilevel genotype–phenotype map. *J Royal Soc Interface* **15**: 20170516.

124. Tarver JE, Taylor RS, Puttick MN, Lloyd GT, Pett W, Fromm B, Schirrmeister BE, Pisani D, Peterson KJ and Donoghue PCJ. 2018. Well-annotated microRNAomes do not evidence pervasive miRNA loss. *Genome Biol Evol* **10**: 1457-1470.

STAR METHODS - *Quantification and Statistical Analysis*

Physiological Data

The masses and *rMR*s of the four thermogenic organs were obtained from the dataset of Wang et al (2012)[1], originally derived from the compilation of Navarette et al (2011)[2] (Supplementary Table S1). Relative brain sizes for the logistic models were obtained from Grabowski et al (2023)[3].

Values for thermal conductance (C_{min}) were obtained from the dataset of Fristoe et al (2015)[4], with substitutions of congeneric species from the dataset of Wang et al (2012)[1]. Where C_{min} was available for two or more congeneric species, we chose the one with the mass closest to the species in the Wang dataset. Body temperatures were obtained from the AnAge database[5].

MicroRNA Families, *Binning*

Complements of conserved microRNA families were obtained from the most complete assembly for each species using the covariance model MirMachine[6], trained on the manually-curated database of microRNA genes, MirGeneDB2.1[7] (Supplementary Tables S1 and S2). For Scandentia, Lagamorpha and Rodentia, *mirFam* refers to the number of families common to Euarchontoglires. For Lorisiformes, Lemuriformes and Platyrrhini, it refers to the number of families shared with Catarrhini. For the original regression of organ *cMR*s on *mirFam* and organ size (Figure 3), *mirFam* was binned according to natural divisions in its distribution: 141 - 161 (Scandentia and Glires), 165 - 181 (Glires, Lemuriformes and Platyrrhini), and 194 - 208 (Catarrhini).

Phylogenetic Trees

Using Mesquite © (2021) we derived ultrametric trees for 51 Euarchontoglires or 24 primates from the phylogenies of Alvarez-Carretero et al (2021)[8] and Shao et al (2023)[9] (Figures 8 and 9, respectively).

Variable Rate Phenograms

Variable rate trees and ancestral node values were inferred using BayesTraits.v4[10-11] (software available at www.evolution.rdg.ac.uk). Bayes factors for variable rate trees were computed from the difference between the median of the top 1% likelihoods and the median likelihood of the 1% of trees with the smallest non-zero sum of changes to branch length, i.e. those trees most similar to the reference time tree, as in Fromm and Sorger (2023)[12]. Phenograms were generated using Phytools[13].

Statistics

Linear, logistic and partial least squares regressions and normal mixture clustering were carried out and visualized using JMP16®. All R^2 values were adjusted for the number of predictors. Phylogenetic linear regressions were carried out using the R: CAPER package[14].

STAR METHODS - *References*

1. Wang ZM, Zhang J, Ying Z and Heymsfield SB. Organ-tissue level model of resting energy expenditure across mammals: new insights into Kleiber's Law. 2012. *ISRN Zool*: 673050.

2. Navarette A, van Schaik CP and Isler K. 2011. Energetics and the evolution of human brain size. *Nature* **480**: 91-93.

3. Grabowski M, Kopperud BT, Tsuboi M and Hansen TF. 2023. Both diet and sociality affect primate brain-size evolution. *Syst Biol* **72**: 404-418.

4. Fristoe TS, Burger JR, Balk MA, Khaliq I, Hof C and Brown JH. 2015. Metabolic heat production and thermal conductance are mass-independent adaptations to thermal environment in birds and mammals. *Proc Natl Acad Sci USA* **112**: 15934-15939.

5. Magalhães JP, Abidi Z, dos Santos GA . . (many others) . . Ka Po To P. 2024. Human Ageing Genomic Resources: updates on key databases in ageing research. *Nucl Acids Res* **52**: D900-D908.

6. Umu SU, Paynter VM, Trondsøn H, Buschmann T, Rounge TB, Peterson KJ and Fromm B. 2023. Accurate microRNA annotation of animal genomes using trained covariance models of curated microRNA complements in MirMachine. *Cell Genomics* **3**: 100348.

7. Fromm B, Høye E, Domanska D, Zhong X, Aparicio-Puerta E, Ovchinnikov V, Umu SU, Chabot, PJ, Kang W, Aslanzadeh M, Tarbier M, Mármol-Sánchez E, Urgese G, Johansen M, Hovig E, Hackenberg M, Friedländer MR and Peterson KJ. 2021. MirGeneDB 2.1: toward a complete sampling of all major animal phyla. *Nucl Acids Res* **50**: D204-D210.

8. Álvarez-Carretero S, Tamuri A, Battini M, Nascimento F, Carlisle E, Asher R, Yang Z, Donoghue P and Dos Reis M. 2022. A species-level timeline of mammal evolution integrating phylogenomic data. *Nature* **602**: 263-267.

9. Shao Y, Zhou, Li F . . (many others) . . Wu DD. 2023. Phylogenomic analyses provide insights into primate evolution. *Science* **380**: 913-924.

10. Pagel M, Meade A and Barker D. 2004. Bayesian estimation of ancestral character states on phylogenies. *Syst Biol* **53**: 673-684.

11. Venditti C, Meade A. and Pagel M. 2011. Multiple routes to mammalian diversity. *Nature* **479**: 393-396.

12. Fromm B and Sorger T. 2023. Rapid adaptation of cellular metabolic rate to the microRNA complements of mammals and its relevance to the evolution of endothermy. *iScience* **27**: 108740.

13. Revell LJ. 2012. phytools: an R package for phylogenetic comparative biology (and other things). *Methods Ecol Evol* **3**: 217-223.

14. Orme D, Freckleton RP, Thomas GH and Petzoldt T. 2013. CAPER: comparative analyses of phylogenetics and evolution in R. *Methods Ecol and Evol* **3**: 141-151.

15. Elia M. 1992. Organ and tissue contribution to metabolic rate. In *Energy Metabolism: Tissue Determinants and Cellular Corollaries*. Kinney JM and Tucker HN (editors), pp: 19–60. Raven Press, New York.

SUPPLEMENTARY INFORMATION

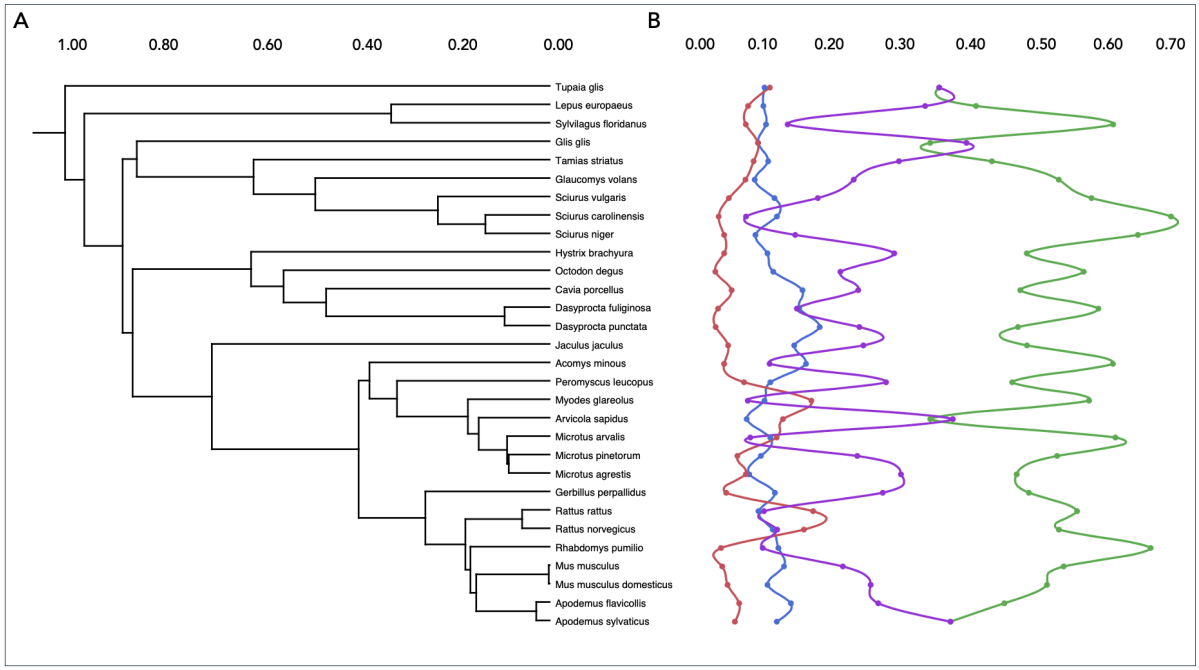

Figure S1. The proportions of brain and liver vary reciprocally in the Euarchontoglires Core. Species include one Scandentia, two Lagomorpha, and 27 Rodentia, including three Sciuridae.
A. Ultrametric phylogenetic tree[8]. The scale represents the relative time of divergence.
B. Mass proportion of each organ relative to total Core mass.

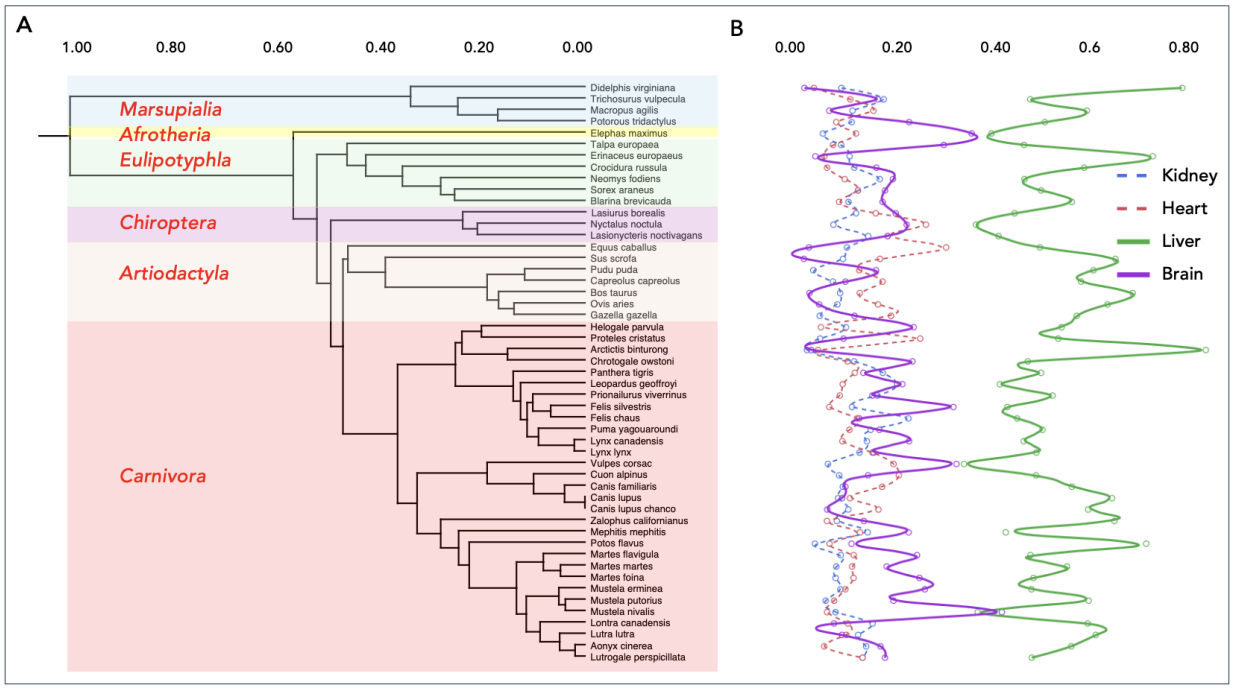

Figure S2. Core organ proportions in Metatheria, Afrotheria, and Laurasiatheria.
A. Ultrametric phylogenetic tree8. The scale represents the relative time of divergence.
B. Mass proportion of each organ relative to total Core mass. Note the difference in range compared to Supplementary Figure S1-B.

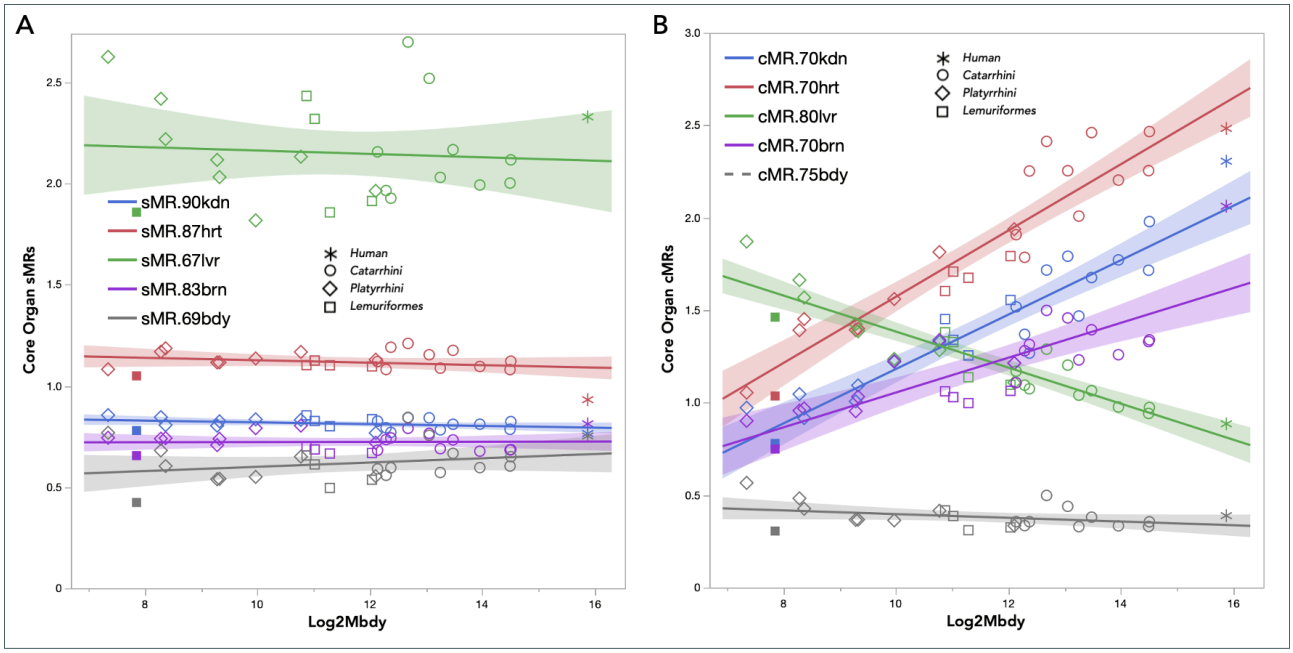

Figure S3. *sMR* slopes are independent of size while *cMR* slopes vary with size.

A. Log-based *sMR* slopes are independent of organ or body size (*N* = 24).

B. *cMR* slopes of Core thermogenic organs and whole-body *cMR* scaled to Kleiber's log-based exponent[39].

Filled symbols represent the heterotherm *Cheirogaleus_medius*.

See the description of Figure 3 for details of the estimation of the Core organ *cMR*s.

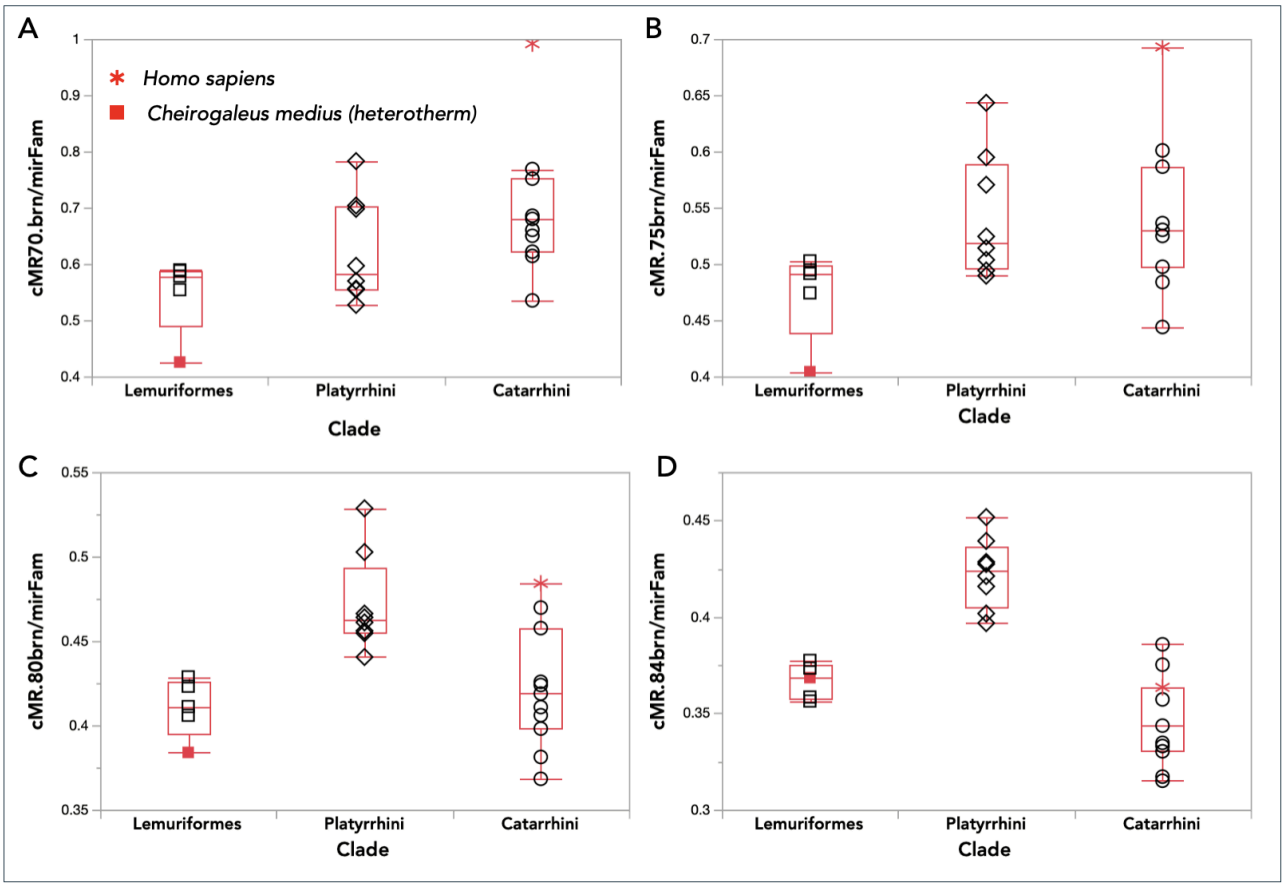

Figure S4. Distributions of the ratios of brain *cMR* or *sMR* to *mirFam* (N = 24).
A: ***cMR.70****brn/mirFam*. B: ***cMR.75****brn/mirFam*. C: ***cMR.80****brn/mirFam*. D: ***sMR.84****brn/mirFam*.
Log *rMRbrn*/log *Mbrn* = 0.84, hence *sMRbrn* = *rMRbrn*/$M^{0.84}$.
Boxplots represent medians, quartiles, minima and maxima.

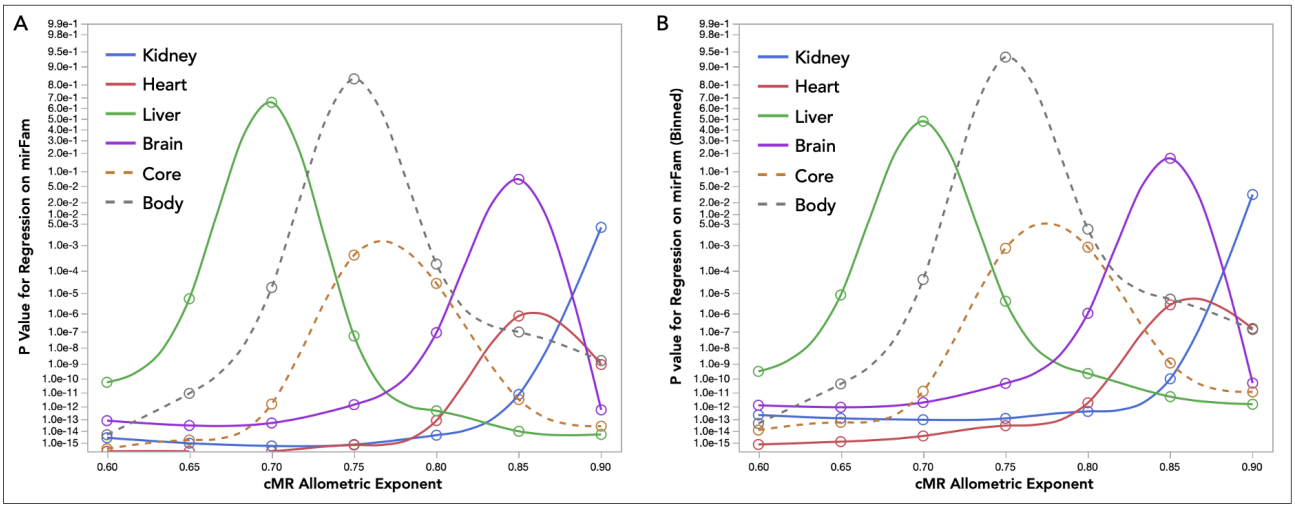

Figure S5. Dependence of *cMR* on *mirFam* or binned *mirFam* without mass correction (51 Euarchontoglires).
A. *P* values for the regression of each *cMR* on *mirFam*. Compare with Figure 3.
B. *P* values for the regression of each *cMR* on binned *mirFam*. *mirFam* was binned according to natural divisions in its distribution: 141 - 161 (Scandentia and Glires), 165 - 181 (Glires, Lemuriformes and Platyrrhini), and 194 - 208 (Catarrhini).

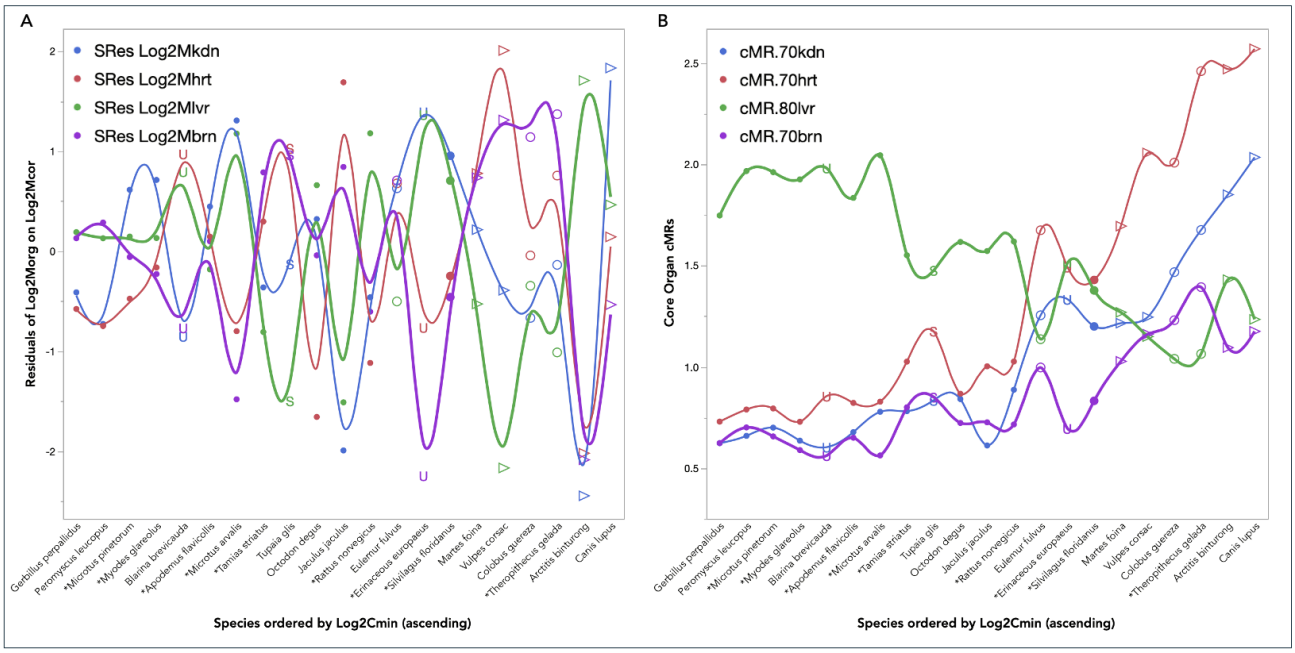

Figure S6. Core organ tradeoffs in Boreoeutheria ordered according to thermal conductance.

A. Reciprocal variation of studentized residuals of each Log_2*Morg* regressed on Log_2*Mcor.*

B. The tradeoff between *cMR.70brn* and *cMR.80lvr* is apparent except among the species with the lowest values of C_{min}. *Asterisks represent species in the 4-organ dataset of Wang et al (2012)[1] that have been substituted for congeneric species in the C_{min} dataset of Fristoe et al (2015)[4].

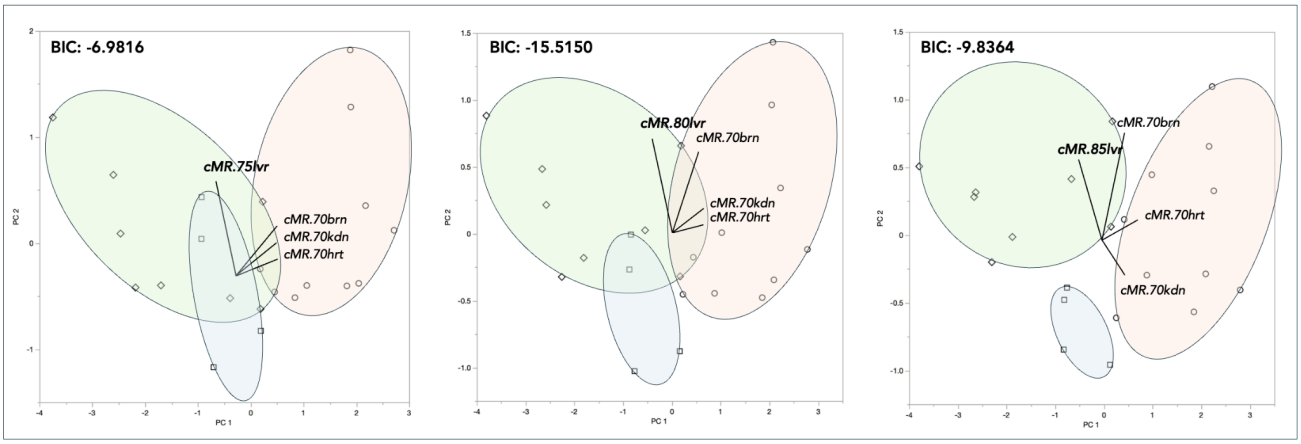

Figure S7. Unsupervised classification of primate clades based on Core *cMR* composition.

Of the four *cMR* models with *VIP* = 4 (Figure 6B), only two (with *cMR.80lvr* and *cMR.85lvr*) resolved Platyrrhini from Lemuriformes. Principal components were calculated from each *cMR* correlation matrix, and membership in two clusters estimated by expectation maximization of their joint probability distributions (normal mixtures algorithm)[43]. BIC: Bayes Information Criterion.

Liver *cMR* was varied between *cMR.75lvr* - *cMR.85lvr* (***bold type***); kidney, heart and brain *cMR* = *cMR.70*. Ellipses were hand-drawn to encompass all members of each phylogenetic clade.

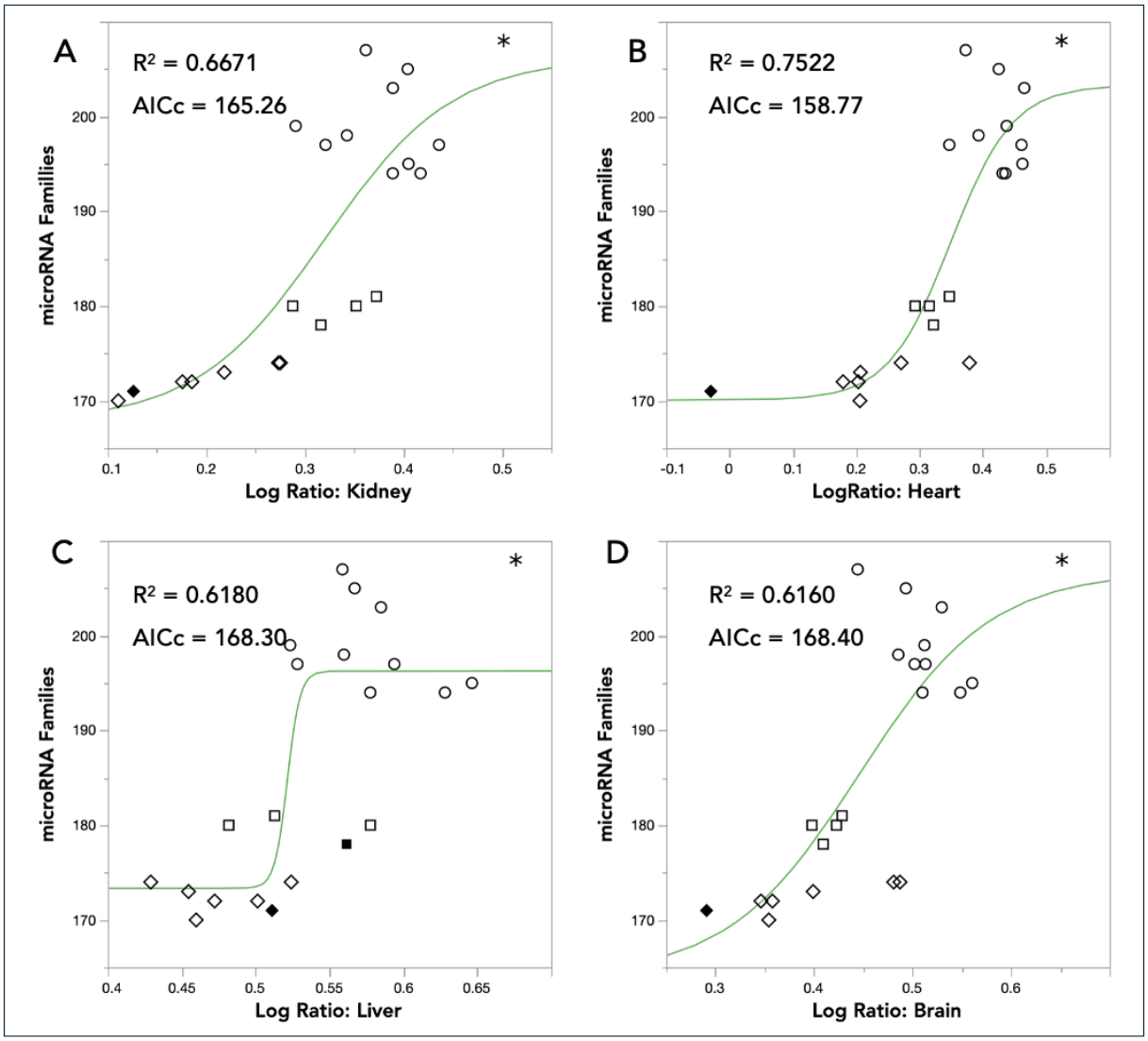

Figure S8. Logistic models for evolution of the relative size of four thermogenic organs. Symbols representing clades as in previous figures, with filled symbols representing heterotherms.

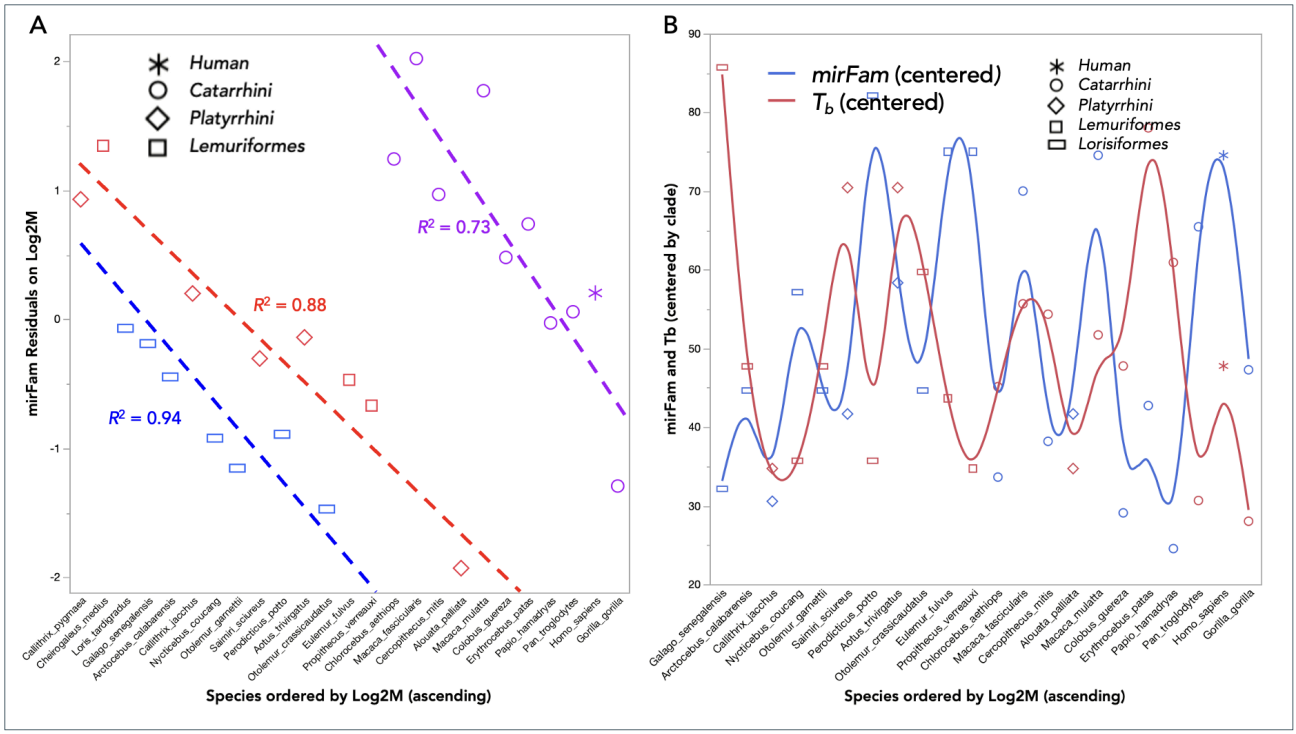

Figure S9. Conservation of *mirFam* and *mirFam* x T_b (range-standardized by clade).
A. The *mirFam*-$\log_2 M$ relationship is least conserved among Catarrhini (purple).
B. Visualization of the reciprocal variation of *mirFam* and T_b. In order to control for phylogeny, the data were range-standardized for Catarrhini, Lorisiformes, and Platyrrhini+Lemuriformes.

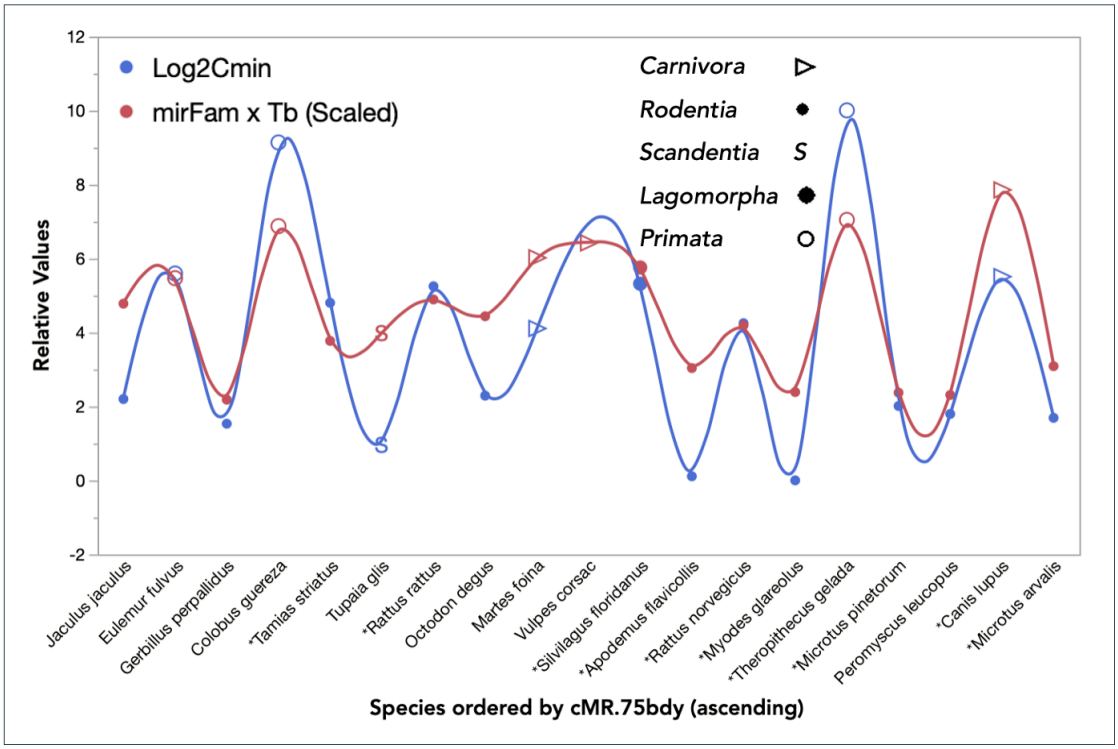

Figure S10. *mirFam* x T_b tracks thermal conductance across Boreoeutheria.
The values of the product *mirFam* x T_b (ºC) were rescaled to the range of $\text{Log}_2 C_{min}$ (N = 19).
*Asterisks represent species in the 4-organ dataset of Wang et al (2012)[1] that have been substituted for congeneric species in the C_{min} dataset of Fristoe et al (2015)[4].

Table S1. Summary of species *mirFam*, mass and resting *MR*s for organs, Core and body. All physiological data were obtained from Wang et al (2012)[1], most of which had been compiled By Navarette et al (2011)[2]. The names of the indicated taxa were substituted with congeneric species on the phylogenies of Álvarez-Carretero et al (2022)[8] and Shao et al (2023)[9].

Clade	Wang Taxon Names	Names on Phylogeny	*mirFam*	*Mkdn* (g)	*Mhrt* (g)	*Mlvr* (g)	*Mbrn* (g)	*Mcor* (g)	*Mbdy* (g)	*MRkdn* (W)	*MRhrt* (W)	*MRlvr* (W)	*MRbrn* (W)	*MRcor* (W)	*MRbdy* (W)
Primates	*Alouatta sara*	*Alouatta palliata*	174	9.9	24	81.2	56.5	171.6	4399.6	13.7088	13.6112	33.6452	12.9948	73.96	169.5872
Primates		*Callithrix jacchus*	172	2.9	2.8	17.8	7.3	30.8	311.8	6.039	17.928	37.352	20.453	81.772	180.7072
Primates	*Cebualla pygmaea*	*Callithrix pygmaea*	171	1.9	0.86	13.5	4.4	20.66	162.66	6.8432	11.1622	29.0377	20.9296	67.9727	112.3625
Primates		*Cheirogaleus medius*	176	1	0.93	6.3	2.8	11.03	231.03	1.5238	0.94858	15.012	2.5432	20.02758	25.77858
Primates		*Chlorocebus pygerythrus*	199	12.1	42.6	89	80.8	224.5	5300.5	2.204	2.8616	16.643	3.8471	25.5557	35.7841
Primates		*Colobus guereza*	198	23.3	37	171	86.5	317.8	9749.8	2.9356	3.5644	14.553	6.2832	27.3362	46.7808
Primates		*Eulemur fulvus*	180	9.5	11.8	43.4	22.5	87.2	2500.2	1.4364	3.3495	13.248	4.0794	22.1133	33.0213
Primates		*Eulemur macaco*	180	14.2	9.1	77.8	24.2	125.3	1875.3	2.2227	3.4817	16.2184	4.78	26.7028	45.6892
Primates	Human	*Homo sapiens*	208	250	320	1700	1300	3570	59970	9.2862	14.1312	40.05	25.56	89.0274	199.0161
Primates	*Hylobates concolor*	*Hylobates pileatus*	195	35.2	58.2	293	137.8	524.2	6550.2	13.3043	25.16	63.612	27.9395	130.0158	323.3718
Primates		*Lemur catta*	178	11.2	11.7	72.9	22.8	118.6	2074.6	12.789	17.135	50.27	15.162	95.356	195.6392
Primates		*Leontopithecus chrysomelas*	173	4.1	3.8	18.9	13.2	40	642	27.4	39.162	78.566	35.518	180.646	471.706
Primates	*Macaca nigra*	*Macaca arctoides*	205	50	61	241	118	470	15870	42.6393	63.242	115.64	49.59	271.1113	669.3613
Primates	Monkey	*Macaca fascicularis*	207	21	23	110	42	196	4500	21.394	51.5696	84.252	44.5244	201.74	419.94
Primates		*Mandrillus sphinx*	194	49.9	76	331	168	624.9	23024.9	0.8932	1.31274	3.9304	2.006	8.14234	13.62034
Primates		*Papio hamadryas*	197	80.3	103	392	174	749.3	23249.3	2.229	2.4725	9.2769	3.8025	17.7809	31.2792
Primates	*Saguinus lagonotus*	*Saguinus midas*	170	1.9	3.3	14.4	7.8	27.4	330.4	0.2841	0.2094	2.2764	0.56832	3.33822	4.47022
Primates		*Saguinus oedipus*	172	3.1	3.7	20.9	10	37.7	623.7	0.23424	0.1456	1.39829	0.2828	2.06093	2.90093
Primates		*Saimiri boliviensis*	174	6.7	6.5	19.4	29	61.6	1002.6	0.609	0.34636	3.7466	0.7304	5.43236	8.15126
Primates		*Sapajus apella*	171	10.4	13.4	49.3	50.8	123.9	1749.9	0.5126	0.25916	3.4181	0.29133	4.48119	5.79399
Primates		*Symphalangus syndactylus*	194	43.7	51.5	294	143	532.2	8500.2	1.179	0.93177	9.5588	1.2834	12.95297	20.57737
Primates		*Theropithecus gelada*	203	38	77.2	236	140.9	492.1	11402.1	0.27412	0.10241	1.43344	0.29232	2.10229	2.94789
Primates		*Trachypithecus vetulus*	197	15.4	19.2	90	72	196.6	4999.6	0.47379	0.21728	3.2058	0.3715	4.26837	5.62837
Primates		*Varecia rubra*	181	22.4	18.1	72.2	35.7	148.4	4200.4	0.25038	0.19992	2.1967	0.44973	3.09673	4.03113
Scandentia		*Tupaia glis*	151	1.1	1.17	3.4	3.4	9.07	141.07	0.31892	0.24768	1.835	0.46055	2.86215	4.13635
Glires		*Acomys minous*	157	0.32	0.18	0.9	0.9	2.3	42.3	0.779	0.98487	6.3756	1.54	9.67947	18.10547
Glires		*Apodemus flavicollis*	141	0.34	0.18	1	0.61	2.13	25.13	7.2688	9.5589	41.0427	9.1884	67.0588	118.8928
Glires		*Apodemus sylvaticus*	155	0.26	0.14	1.1	0.57	2.07	18.07	6.0705	9.4282	23.219	8.82	47.5377	109.5518
Glires		*Arvicola sapidus*	149	0.7	0.28	2.6	1.1	4.68	61.68	9.301	7.5257	44.9684	9.8736	71.6687	118.9187
Glires	Guinea Pig	*Cavia porcellus*	174	5.6	2.3	27	4.7	39.6	799.6	4.623	5.785	13.2502	12.934	36.5922	64.7281
Glires		*Gerbillus perpallidus*	147	0.27	0.13	1	0.58	1.98	29.98	110	140.8	340	312	902.8	1489.36
Glires		*Glaucomys volans*	176	0.59	0.56	2.9	1.9	5.95	54.95	20.768	41.4966	121.302	47.1276	230.6942	362.6636
Glires		*Glis glis*	168	0.68	0.48	3.2	1.5	5.86	83.86	25.2149	35.5865	113.484	47.047	221.3324	388.6604
Glires		*Jaculus jaculus*	158	0.29	0.45	1.1	1.2	3.04	48.04	7.26	31.1406	38.982	28.4416	105.8242	221.0494
Glires		*Lepus europaeus*	173	18.5	28.9	90.4	14.8	152.6	3338.6	26.4969	46.74	97.645	48.048	218.9299	617.6499
Glires		*Microtus agrestis*	148	0.17	0.12	0.63	0.39	1.31	15.31	11.544	22.3108	44.748	5.5648	84.1676	162.2246
Glires		*Microtus arvalis*	153	0.55	0.19	1.9	0.39	3.03	27.03	4.3533	4.2864	22.048	3.5392	34.2269	61.949
Glires		*Microtus pinetorum*	154	0.36	0.15	1.1	0.58	2.19	21.19	0.57664	0.57312	4.256	0.954	6.35976	9.89316
Glires		*Mus musculus*	167	0.28	0.07	0.68	0.36	1.39	15.39	0.67473	0.76758	3.6366	1.4784	6.55731	10.79621
Glires	Mouse	*Mus musculus domesticus*	167	0.51	0.16	1.8	0.5	2.97	27.97	0.51802	0.70224	4.3094	1.2825	6.81216	9.19356
Glires		*Myodes glareolus*	143	0.24	0.1	0.67	0.35	1.36	15.36	1.3056	1.7629	5.3185	3.3831	11.7701	21.4049
Glires		*Octodon degus*	156	1.1	0.41	4.8	1.9	8.21	129.21	2.304	2.6488	12.8904	3.6075	21.4507	39.9589
Glires		*Peromyscus leucopus*	160	0.3	0.15	1.2	0.74	2.39	22.39	0.8998	0.46494	5.6736	1.1343	8.17264	13.26674
Glires		*Rattus norvegicus*	168	1.5	0.87	9.2	2.3	13.87	209.87	3.9368	2.1022	19.602	2.1667	27.8077	51.4437
Glires	Rat	*Rattus rattus*	167	2.8	1.1	14.3	1.9	20.1	390.1	0.25752	0.57375	1.6973	0.8256	3.35417	5.59067
Glires		*Rhabdomys pumilio*	161	0.41	0.21	1.8	0.6	3.02	50.02	0.28704	0.23274	1.4337	0.63	2.58348	4.61148
Glires		*Sciurus carolinensis*	175	3.2	2.8	16.4	7.5	29.9	595.9	0.34272	0.21075	2.1175	0.44892	3.11989	4.20479
Glires		*Sciurus niger*	165	3	2.5	10.7	7.5	23.7	412.7	0.16592	0.17472	1.31481	0.31512	1.97057	2.81057
Glires		*Sciurus vulgaris*	175	1.7	1.7	5.5	6.3	15.2	274.2	0.24948	0.17511	1.748	0.4263	2.59889	4.10249
Glires		*Sylvilagus floridanus*	170	6.3	4.8	32	7.9	51	972	2.0888	1.0945	12.584	0.9709	16.7382	29.7252
Glires		*Tamias striatus*	173	0.81	0.66	2.9	2.4	6.77	103.77	0.36285	0.26607	2.7414	0.4098	3.78012	6.09722

Table S2. Primate microRNA families, brain volume, body mass and temperature.
Endocranial volume (ECV) and body mass were obtained from Grabowski et al (2023)[3].
Body temperatures were retrieved from the AnAge database (Magalhães et al, 2024)[5].

Order	Species	*mirFam*	ECV	Mass (g)	T_b (°C)
Catarrhini	*Homo sapiens*	208	1252.00	50000	37.0
Catarrhini	*Pan troglodytes*	206	368.35	44967	35.7
Catarrhini	*Gorilla gorilla*	202	490.41	120950	35.5
Catarrhini	*Macaca fascicularis*	207	63.98	4251	37.6
Catarrhini	*Macaca mulatta*	208	88.98	6793	37.3
Catarrhini	*Papio hamadryas*	197	146.17	14150	38.0
Catarrhini	*Chlorocebus aethiops*	199	65.00	3720	36.8
Catarrhini	*Erythrocebus patas*	201	97.73	9450	39.3
Catarrhini	*Cercopithecus mitis*	200	71.33	6109	37.5
Catarrhini	*Colobus guereza*	198	74.39	8589	37.0
Platyrrhini	*Callithrix jacchus*	172	7.24	320	36.0
Platyrrhini	*Callithrix pygmaea*	171	4.17	116	35.2
Platyrrhini	*Aotus trivirgatus*	177	16.85	989	38.0
Platyrrhini	*Saimiri sciureus*	174	24.14	799	38.0
Platyrrhini	*Alouata palliata*	174	49.88	6250	36.0
Lemuriformes	*Eulemur fulvus*	180	25.77	2292	36.5
Lemuriformes	*Cheirogaleus medius*	176	2.60	140	38.0
Lemuriformes	*Propithecus verreauxi*	180	26.21	2955	36.0
Lorisiformes	*Otolemur garnettii*	166	11.50	764	36.0
Lorisiformes	*Otolemur crassicaudatus*	166	11.78	1150	36.6
Lorisiformes	*Galago senegalensis*	165	3.96	194	37.9
Lorisiformes	*Loris tardigradus*	166	5.87	193	35.5
Lorisiformes	*Nycticebus coucang*	167	10.13	653	35.4
Lorisiformes	*Arctocebus calabarensis*	166	6.92	309	36.0
Lorisiformes	*Perodicticus potto*	169	12.42	835	35.4

Table S3. Parameters of the thermodynamic Core *cMR* models for three clades of Boreoeutheria.
Brain mass, body mass and *rMR* data were obtained from the dataset of Wang et al (2012)[1].
For the median, average and log ratios of brain to body, mass values were expressed in mg.
K = Kidney, H = Heart, L = Liver and B = Brain.

Clade	*N*	Mbdy (g) (median)	Mbrn/ Mbdy	Log_2*Mbrn*/ Log_2*Mbdy*	Core *cMR* Exponent	Core Model R^2	Model Organ Coefficients				Model Organ VIP Values			
							K	H	L	B	K	H	L	B
Carnivora	30	5100	0.0084	0.6918	0.60	96.6015	0.496	0.672	0.297	0.060	1.060	1.158	0.866	0.887
Primates	22	4300	0.0136	0.7130	0.53	98.0708	0.531	0.689	0.367	0.088	1.076	1.057	0.894	0.961
Catarrhini	10	9125	0.0108	0.7182	0.60	99.3394	0.4965	0.4058	0.2703	0.2192	1.1111	1.1756	0.407	1.1035
Platyrrhini	8	632.85	0.0235	0.7074	0.40	90.7004	0.7111	1.1248	0.4986	-0.396	0.9414	1.1213	0.9606	0.9663
Glires	26	52	0.0188	0.6381	0.40	99.0760	0.638	0.489	0.030	-0.130	1.179	1.089	0.873	0.813

Table S4. Phylogenetic regressions of primate organ *cMR*s on *mirFam* (*N* = 22).
The dataset excluded two outliers (the human and the heterotherm *Cheriogaleus medius*).
For reference, see the logistic regressions of *mirFam* on relative organ size (Supplementary Figure S8).

	Allometric Exponent	Pagel's *lambda*	R^2	*P*	*AICc*
KIDNEY	0.80	0	0.5366	6.39E-05	-42.7
	0.75	0	0.5834	2.14E-05	-20.09
	0.70	0	0.5958	1.56E-05	-0.93
	0.65	0	0.5946	1.61E-05	16.22
	0.60	0	0.5859	2.00E-05	32.13
		Pagel's *lambda*	R^2	*P*	*AICc*
HEART	0.80	0	0.4937	1.60E-04	-38.02
	0.75	0	0.6476	3.83E-06	-17.88
	0.70	0	0.6962	8.44E-07	0.63
	0.65	0	0.7133	4.69E-07	17.65
	0.60	0	0.7163	4.21E-07	33.66
		Pagel's *lambda*	R^2	*P*	*AICc*
LIVER	0.80	0	0.5724	2.79E-05	-15.22
	0.75	0	0.4011	9.28E-04	-10.98
	0.70	0	0.0854	1.01E-01	-2.86
	0.65	0	-0.0344	5.89E-01	10.24
	0.60	0.962	0.0145	2.66E-01	27.34
		Pagel's *lambda*	R^2	*P*	*AICc*
BRAIN	0.80	1	0.0329	2.05E-01	-63.9
	0.75	1	0.107	7.55E-02	-35.75
	0.70	1	0.1336	5.07E-02	-10.58
	0.65	1	0.151	4.17E-02	11.76
	0.60	1	0.1596	3.71E-02	32.24